

# Effect of structural characteristics on functional properties of textured vegetable proteins

Thiemo van Esbroeck<sup>a</sup>, Guido Sala<sup>a</sup>, Markus Stieger<sup>b,c</sup>, Elke Scholten<sup>a,\*</sup>

<sup>a</sup> Department of Physics and Physical Chemistry of Foods, Wageningen University & Research, Bornse Weilanden 9, 6708WG, Wageningen, the Netherlands

<sup>b</sup> Division of Human Nutrition and Health, Wageningen University & Research, Bornse Weilanden 9, 6708WG, Wageningen, the Netherlands

<sup>c</sup> Department of Food Quality and Design, Wageningen University & Research, Bornse Weilanden 9, 6708WG, Wageningen, the Netherlands

## ARTICLE INFO

### Keywords:

Meat analogues  
Plant protein  
X-ray microtomography  
Microstructure  
Porosity  
Texture

## ABSTRACT

Meat analogues are predominantly composed of a pre-structured form of protein called textured vegetable protein (TVP) that is designed to mimic the fibrous structure of animal muscle meat. Limited information is available regarding the link between structural characteristics of TVPs and their functional properties. This study investigated the relationships between the structural characteristics of commercial TVPs and (a) their rehydration behaviour, as well as (b) the mechanical properties and serum release (cooking loss and expressible liquid) of patties prepared from these TVPs. The micro- and macrostructural features of thirteen commercial TVPs were quantified using X-ray microtomography. Apparent density (205–1042 kg m<sup>-3</sup>), porosity (27.1–80.9%), pore size (251–4790 μm), wall thickness (108–657 μm), and wall density (597–1515 kg m<sup>-3</sup>) varied largely across samples. In the early stages of water absorption, thicker walls promoted the absorption of larger volumes of water. In contrast, the maximum water absorption capacity as well as water holding capacity were higher for TVPs with thinner walls and higher porosity, highlighting the impact of structural features of TVPs on water absorption during rehydration. Significant positive correlations between cooking loss and expressible liquid indicated that patties with higher serum release during cooking also tended to release more during compression. TVPs with thicker walls resulted in stiffer patty batters, and TVPs with smaller pores resulted in stiffer grilled patties. We conclude that the structural characteristics of TVPs influence their rehydration behaviour and various functional properties of patties made with them.

## 1. Introduction

The consumption of plant-based meat products has strongly increased over the last years due to growing awareness and concerns about environmental, health-related and animal welfare issues related to meat consumption (Attwood & Hajat, 2020; Cheah et al., 2020; Dagevos & Voordouw, 2013; De Backer & Hudders, 2014; European Commission, 2005; Hoek et al., 2011; Lacroix & Gifford, 2019; Mayfield et al., 2007; McEachern & Schröder, 2002; Steinfeld et al., 2006). As a result, consumers are increasingly willing to decrease meat consumption and try out plant-based alternatives, although this transition is still slow (Cheah et al., 2020; Dagevos & Verbeke, 2022). This has led to advancements in the development of meat analogues in recent years. Meat analogues (also referred to as fake meat, imitation meat, mock meat or meat substitutes (Ismail et al., 2020; Joshi & Kumar, 2015)) are “meat-like food products made from plant-based ingredients, and are

designed to mimic the appearance, texture, and nutritional content of real meat products” (Chiang et al., 2021). Such products will be crucial for facilitating the protein transition, especially in Western countries (Elzerman et al., 2011; Hoek et al., 2011). Despite recent improvements in texture and flavour, the sensory characteristics of meat analogues are often still suboptimal (Boukid, 2020).

The majority of meat analogues typically consist of 60% protein in a pre-structured form, so-called textured vegetable protein (TVP) (Kyriakopoulou et al., 2021). For products such as sausages and burger patties, TVP is rehydrated and mixed with fat and binding agents to create structures that mimic meat products (Kyriakopoulou et al., 2021). Serum release properties of meat analogues are very important, as they encompass the liquid expelled during cooking and consumption, and thereby impact sensory properties. These product properties are greatly influenced by the water absorption capacity (WAC) and water holding capacity (WHC) of TVP (Hong et al., 2022; Tuohy, 1980). Insights into

\* Corresponding author.

E-mail address: [elke.scholten@wur.nl](mailto:elke.scholten@wur.nl) (E. Scholten).

<https://doi.org/10.1016/j.foodhyd.2023.109529>

Received 13 September 2023; Received in revised form 26 October 2023; Accepted 8 November 2023

Available online 15 November 2023

0268-005X/© 2023 The Authors. Published by Elsevier Ltd. This is an open access article under the CC BY license (<http://creativecommons.org/licenses/by/4.0/>).

the relationships between TVP structural properties and WAC and WHC are lacking, since studies that included characterisation of the microstructure of TVP did not investigate water absorption, and vice versa (Yu et al., 2013; Zhou et al., 2021). We hypothesize that water absorption capacity (WAC) and water holding capacity (WHC) of TVPs are related to the structural characteristics of TVPs.

The structural characteristics of TVPs are mostly determined by the low-moisture extrusion (LME) process that is used to produce them. During low-moisture extrusion, protein flours, concentrates or isolates are structured by shear alignment and subsequent crosslinking of the different phases in the melt. The resulting TVP structures can differ considerably in porosity, pore size and wall thickness, depending on the expansion of the material during processing and the type of raw materials used. Many studies reported the influence of extrusion conditions on structural characteristics of the TVPs (Brishti et al., 2021; Samard et al., 2019, 2021; Samard & Ryu, 2019a, 2019b). Brishti et al. (Brishti et al., 2021) studied the extrusion conditions for the texturisation of mung bean protein, and found that the moisture content in the feed had the largest impact on TVP properties, followed by barrel temperature and screw speed. The raw materials also considerably affect TVP properties, as shown by Samard et al. (Samard et al., 2019), who reported that wheat gluten strongly enhanced textural properties of extruded soy protein isolate.

Although changing the extrusion feed and processing conditions have been widely used to tune the functional properties of TVPs, few studies explored the structural characteristics of TVPs that underlie functional properties. Scanning electron microscopy is a common technique used to visualise the structure of TVP, but usually only qualitative information is obtained. Instead, quantitative information can be obtained with X-ray tomography (XRT). In recent years, XRT has been used to characterise the microstructure of extruded snacks (Agbisit et al., 2007; Beck et al., 2018; Chanvrier et al., 2015; Guillemic et al., 2021; Luo et al., 2020) to quantify structural features such as porosity, wall thickness, and pore size, shape and interconnectivity. XRT has not yet been utilised for the characterisation of TVPs, although it could be used to establish relationships between the structural characteristics of TVPs and water absorption and water holding properties.

The structure of TVPs strongly influences serum release, but also the mechanical properties of meat analogues. Samard et al. (Samard et al., 2021) characterised patties obtained from TVPs made under different extrusion conditions. TVPs made with a higher moisture content during extrusion resulted in patties with higher springiness, cohesiveness, hardness and cutting strength. The authors suggested that a stronger protein network was formed at higher moisture contents. An increase in die temperature resulted in a decrease in springiness and cohesiveness of the patties, explained with the same reasoning.

Hong et al. (Hong et al., 2022) studied 28 commercial TVPs from different manufacturers and protein types and found that hardness of patties was lower when WAC of the TVP was higher. This was consequently linked to serum release, as both cooking loss and expressible liquid of patties were negatively correlated with the WAC of the TVP. These differences may just be related to the initial water content in the patties, as TVPs were rehydrated up to the maximum WAC, and therefore patties had different moisture contents. The link with the structural characteristics of the TVP could therefore not be obtained. To summarize, the relationships between structural characteristics of TVP and rehydration behaviour and functional properties of patties are still underexplored.

The aims of this study were (a) to quantify structural characteristics of commercially available TVPs and (b) to relate structural characteristics to water absorption and water holding behaviour and functional properties of patties. A set of 13 commercially available TVPs produced with low-moisture extrusion was used, and porosity, pore size and wall thickness were quantified using XRT. These structural features were correlated to the water absorption rate, water absorption capacity, and the water holding capacity. Patties were prepared from all TVPs to

determine the influence of structural characteristics of TVPs on functional properties of patties, including cooking loss, expressible liquid and textural and rheological properties. The results of this study could help to determine desired structural features of TVPs, and facilitate optimisation of the production process.

## 2. Materials and methods

### 2.1. Materials

Thirteen commercially available textured vegetable proteins (TVP) from three suppliers were used: TP70G, T70S, TP65M, TP-C and TF-C were obtained from Roquette Frères S.A (Lestrem, France); Pea Flakes SVP, Wheat Flakes SVP, Soy Flakes and Soy Chunks XL from the VITA-TEX® range and Flakes FP 76 and Flakes 4080 from the WHEATMEAT® range were kindly provided by GoodMills Innovation GmbH (Hamburg, Germany); Soy granules (Soja Granulat) and soy strips (Soja Geschnetzeltes) were obtained from Vegafit (Deventer, The Netherlands). The TVPs were all produced using low-moisture extrusion and selected to encompass a wide range of structural characteristics. The commercial name, supplier, sample code, source and protein content according to the supplier of all commercial TVPs is given in Table 1. Methylcellulose (Methocel A4M) was purchased from Labshop (Apeldoorn, The Netherlands). Pea protein isolate (PPI) (NUTRALYS® F85M) was obtained from Roquette Frères S.A., (Lestrem, France). Sunflower oil and sodium chloride were purchased from a local supermarket (Jumbo, Wageningen, The Netherlands).

### 2.2. TVP characterisation

#### 2.2.1. Protein content

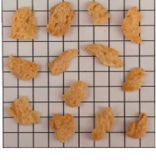
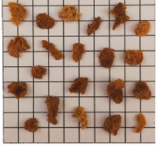
To determine the protein concentration of the TVPs, the elemental nitrogen content of all TVPs was determined using the Dumas method. TVP samples were ground into a powder using a Waring blender (model 8011 ES, Torrington, Connecticut, USA) and nitrogen concentrations were determined during combustion in a Flash EA 1112 N/protein analyser (Thermo Fisher Scientific, Waltham, Massachusetts, USA). A factor of 5.7 was used to convert the nitrogen content to protein content, which is expressed on dry matter basis. Measurements were done in triplicate.

#### 2.2.2. X-ray microtomography (XRT)

The internal structure of TVP pieces was analysed using X-ray microtomography (XRT) using a General Electric Phoenix v|tome|x m (General Electric Co., Wunstorf, Germany). A 240 kV microfocus tube with a tungsten target was employed, and X-rays were produced with a voltage of 90 kV and a current of 100  $\mu$ A. A 0.1 mm Cu filter was used to avoid beam hardening. Images were recorded by a GE DXR detector array with 2024  $\times$  2024 pixels (pixel size 200  $\mu$ m). The detector was located 815 mm from the X-ray source. TVP pieces were loaded into the middle of a 50 mL centrifuge tube (diameter = 30 mm) and placed between two pieces of styrofoam to prevent the sample from moving during the measurement. The apparent volume taken up by TVP was between 5 and 15 cm<sup>3</sup>, depending on the size of the TVP chunks. The sample was placed 58.62 mm from the X-ray source, resulting in a spatial resolution of 15.00  $\mu$ m. The sample was placed on a rotary stage to allow a full scan consisting of 1500 projections over 360°, with a step ratio of 0.24°. The final projection was the average of three images where every image was obtained over 150 ms exposure time. GE reconstruction software version 2.10.1 - RTM (Wunstorf, Germany) was used to calculate the 3D structure via back projection. The reconstructed 3D images were analysed using Avizo imaging software version 2021.2 (Thermo Scientific, Waltham, Massachusetts, USA). The porosity was calculated as the volume of air within the total volume occupied by TVP chunks. The pore size and wall thickness were determined using thickness analysis. At each voxel within the selected 3D structure (either pore

**Table 1**

Sample code (1), commercial name (2), supplier (3), source (4) and protein content according to the supplier (5) of the commercial TVPs used in this study. Images are for TVP visualisation and each square represents 5 mm.

TVP information	Picture of TVPs	TVP information	Picture of TVPs
<ol style="list-style-type: none"> <li>1. ROQ1</li> <li>2. Roquette Frères S.A</li> <li>3. NUTRALYS® TP70G</li> <li>4. Yellow pea</li> <li>5. 72.9% protein</li> </ol>		<ol style="list-style-type: none"> <li>1. GMI1</li> <li>2. GoodMills Innovation GmbH</li> <li>3. VITATEX® Soy Flakes</li> <li>4. Soy bean</li> <li>5. 50.0% protein</li> </ol>	
<ol style="list-style-type: none"> <li>1. ROQ2</li> <li>2. Roquette Frères S.A</li> <li>3. NUTRALYS® T70S</li> <li>4. Yellow pea</li> <li>5. 71.4% protein</li> </ol>		<ol style="list-style-type: none"> <li>1. GMI2</li> <li>2. GoodMills Innovation GmbH</li> <li>3. VITATEX® Soy Chunks XL</li> <li>4. Soy bean</li> <li>5. 50.0% protein</li> </ol>	
<ol style="list-style-type: none"> <li>1. ROQ3</li> <li>2. Roquette Frères S.A</li> <li>3. NUTRALYS® TP-C</li> <li>4. Yellow pea</li> <li>5. 73.2% protein</li> </ol>		<ol style="list-style-type: none"> <li>1. GMI3</li> <li>2. GoodMills Innovation GmbH</li> <li>3. VITATEX® Wheat Flakes SVP</li> <li>4. Wheat + yellow pea</li> <li>5. 74.0% protein</li> </ol>	
<ol style="list-style-type: none"> <li>1. RO4</li> <li>2. Roquette Frères S.A</li> <li>3. NUTRALYS® TF-C</li> <li>4. Fava bean</li> <li>5. 63.2% protein</li> </ol>		<ol style="list-style-type: none"> <li>1. GMI4</li> <li>2. GoodMills Innovation GmbH</li> <li>3. VITATEX® Pea Flakes SVP</li> <li>4. Wheat</li> <li>5. 79.7% protein</li> </ol>	
<ol style="list-style-type: none"> <li>1. ROQ5</li> <li>2. Roquette Frères S.A</li> <li>3. NUTRALYS® TP65M</li> <li>4. Yellow pea</li> <li>5. 68.7% protein</li> </ol>		<ol style="list-style-type: none"> <li>1. GMI5</li> <li>2. GoodMills Innovation GmbH</li> <li>3. WHEATMEAT® Flakes 4080</li> <li>4. Wheat</li> <li>5. 74.0% protein</li> </ol>	
<ol style="list-style-type: none"> <li>1. VEG1</li> <li>2. Vegafit</li> <li>3. Soja Granulat</li> <li>4. Soy bean</li> <li>5. 66.0% protein</li> </ol>		<ol style="list-style-type: none"> <li>1. GMI6</li> <li>2. GoodMills Innovation GmbH</li> <li>3. WHEATMEAT® Flakes 4080</li> <li>4. Wheat</li> <li>5. 76.8% protein</li> </ol>	
<ol style="list-style-type: none"> <li>1. VEG2</li> <li>2. Vegafit</li> <li>3. Soja Geschnetzeltes</li> <li>4. Soy bean</li> <li>5. Unknown</li> </ol>			

space or walls), the maximum possible diameter of a sphere containing that voxel, while staying within the structure, was calculated. Lognormal distributions were fitted to the surface-weighted pore size and wall thickness distributions, from which the mean and variance were calculated. Throughout this study, we refer to the mean pore size (MPS) and mean wall thickness (MWT) along with their variances ( $\sigma_{PS}^2$  and  $\sigma_{WTT}^2$ , respectively). All measurements were performed in triplicate.

### 2.2.3. Density measurements

The apparent density ( $\rho_{app}$ ) of TVP pieces was determined using a displacement method. A known mass of TVP pieces was submerged in a known volume of fine sand, and this was well-mixed to ensure complete surface coverage of the TVP pieces by the sand. Subsequently, the volume of sand displaced by the TVP pieces was measured. It was verified that the sand entering the TVP through its surface openings did not significantly affect the measurement. Measurements were performed in triplicate to obtain mean values and a standard error.

The absolute density ( $\rho_{abs}$ ) of the TVP pieces was measured using an automatic density analyser (ULTRAPYC 1200e, Quantachrome GmbH, Germany). TVP pieces were ground into a powder, weighed into the sample chamber, and after analysis, the  $\rho_{abs}$  values were recorded. Measurements were performed in duplicate.

Based on  $\rho_{app}$  and  $\rho_{abs}$ , the porosity ( $\Phi$ ) of the TVP pieces was calculated as:

$$\Phi_{density} = \frac{\rho_{app} - \rho_{abs}}{\rho_{abs}} \quad (1)$$

At sub-micron level, pores may also be present within the walls smaller than the resolution of XRT. To gain insight into these pores, the wall density,  $\rho_{wall}$ , was calculated as:

$$\rho_{wall} = \frac{\rho_{app}}{\left(1 - \frac{\Phi_{XRT}}{100}\right)} \quad (2)$$

where  $\rho_{app}$  is the apparent density of the TVP and  $\Phi_{XRT}$  the porosity of TVP obtained from XRT measurements.

### 2.2.4. Water absorption capacity

The water absorption capacity (WAC) was measured for all intact TVPs. Twenty grams of TVP were allowed to rehydrate in excess water for 30 min and were gently mixed every 5 min. After 30 min, the TVP was drained on a sieve with a 1 mm mesh. The WAC was calculated as:

$$WAC = \frac{m_a - m_b}{m_b} \cdot 100\% \quad (3)$$

where  $m_a$  is the mass of the rehydrated TVP after draining, and  $m_b$  is the mass of dry TVP. The rehydration water was dried in an oven (Venticell, BMT Medical Technology, Brno, Czech Republic) at 105 °C to determine the dry matter content in the rehydration water. Both masses  $m_a$  and  $m_b$  were corrected for the loss of dry matter in the rehydration water. All measurements were performed in duplicate.

### 2.2.5. Water absorption rate

The water absorption rate was determined for all intact TVPs. Twenty grams of TVP were allowed to rehydrate in excess water. After 1, 2, 5, 10 and 20 min of rehydration, the TVP was drained on a sieve with a 1 mm mesh, and weighed. The amount of water that was absorbed ( $w$ ) at every time interval was calculated using Equation (4). The data were fitted to a two term exponential model of the form

$$w = a(e^{b_1 t} - e^{b_2 t}) \quad (4)$$

to extract different parameters representing the kinetics of water uptake. This model is a simplification of the parallel exponential kinetics (PEK) model introduced by Kohler et al. (Kohler et al., 2003). In our model, the water is assumed to flow into a single "pool" with a maximum value  $a$  in

time  $t$ , with two specific rate constants  $b_1$  and  $b_2$ . In this case, these mechanisms are related to a fast ( $b_1$ ) and a slow ( $b_2$ ) water uptake process. The experimental data was also fitted to various other models including the logarithmic (Karizaki, 2016), two-term (Henderson, 1974), Peleg (Peleg, 1988) and Weibull (Vishwakarma et al., 2013) models. However, Equation (4) is the one that fit best with the experimental data and uses the least parameters.

### 2.2.6. Water holding capacity

The water holding capacity (WHC) was determined for intact and ground TVP samples. Intact or ground TVP was dispersed in water equal to the maximum WAC of intact TVP and allowed to rehydrate at room temperature for 30 min. Subsequently, the samples were centrifuged at 200 g for 15 min in a centrifuge tube with a polypropylene filter insert (filter  $\varnothing = 25.9$  mm, H = 54.5 mm, pore size 1.1 mm). Two filter papers (Whatman 5, qualitative filter paper) were cut to fit the insert and placed in the insert to prevent TVP from permeating the filter. During centrifugation, expelled water permeated the filters and was collected as filtrate. After centrifugation, the TVP was weighed to determine the mass of the water remaining in the TVP. The WHC was calculated as:

$$WHC = \frac{m_c - m_d}{m_d} \cdot 100\% \quad (5)$$

where  $m_c$  is the mass of TVP after centrifugation and  $m_d$  is the mass of dry TVP. All measurements were done in duplicate. In the WHC experiments with ground TVP, we assumed that the ground TVP particles were packed at a maximum packing density for monodisperse spheres of approximately 74% based on the Kepler conjecture (Hales, 2006). Therefore, we assumed that 26% of the water retained by the ground TVP was not held by the powder, but in voids in between the particles.

### 2.2.7. Differential scanning calorimetry (DSC)

The bound water content of all TVPs were measured using differential scanning calorimetry (Discovery DSC-25, TA Instruments, Delaware, USA) based on a method described by Chen and Zhang et al. (Chen et al., 2010) and Hayashi et al. (Hayashi et al., 1992), with some adjustments. Ground TVP was mixed with water to create samples with moisture contents ranging from 30 to 60%. About 20–30 mg of each sample was encapsulated into a hermetically sealed aluminium DSC-pan. The samples were cooled from 20 °C to –50 °C, held at 50 °C for 3 min, and then heated to 40 °C. Heating and cooling were done at 5 °C·min<sup>-1</sup>. The endothermic enthalpy ( $\Delta H$ , J/g) of the melting of water was determined using Trios software version 2.0. The enthalpy and the heat of fusion of water at 0 °C (334 J/g) were used to calculate the free water content in the samples. All measurements were done in duplicate. The free water content was plotted versus the moisture content of samples. The best linear fit through the data points was used to determine the intercept on the x-axis. This value represents the maximum moisture content TVP can hold without the presence of freezable water, which is taken as a measure of the bound water content of the TVP.

## 2.3. Preparation and characterisation of patties

### 2.3.1. Patty preparation

Patties were prepared using the thirteen TVPs, water, sunflower oil

**Table 2**  
Recipe for the preparation of the studied patties.

Ingredient	Content (w/w (%))
TVP	20
Water	57.2
MC	2
PPI	5
NaCl	0.8
SFO	15

(SFO), methylcellulose (MC), pea protein isolate (PPI) and NaCl. The recipe, including the concentrations of all ingredients, is presented in Table 2.

Two types of patties were prepared in this study. In the first type, intact TVP chunks were rehydrated and blended to a size of  $\pm 5$  mm. In the second type, dry TVP was incorporated as a finely-ground powder, to remove the effect of structure, and thereby isolate the effect of TVP composition. For all patties, the dry TVP was rehydrated with water (1:2 by weight) for 30 min and mixed every 10 min. In the case TVP was intact, it was then blended using a Thermomix TM31 (Vorwerk Elektrowerke GmbH & Co. KG, Wuppertal, Germany) at speed 4 to reduce its size to  $\pm 5$  mm. Next, for all types of patties, the other dry ingredients (MC, PPI and NaCl) were mixed into the hydrated and blended TVP for 1 min at a speed of 1.5. The remaining water (17.2 g/100 g patty batter) was then added and the mixture was stirred for an additional minute. This was followed by oil addition and mixing for 1 min. The sides of the mixing bowl were scraped, and the patty batter was mixed for an additional minute. All mixing steps were performed at a speed of 1.5, but in some cases, the mixing speed was briefly increased to 4 when necessary to break up large lumps.

The patty batter was transferred to a SafeLoc® freezer bag (Toppits, Minden, Germany) and refrigerated at 4 °C for at least 12 h. The batter was shaped into patties of 100 g each with a diameter of 70 mm and a thickness of 20 mm using a plastic patty shaper. The patties were placed in a SafeLoc® bag. Air was allowed to escape the bag, after which the bags were closed. The bags were then transferred to a water bath kept at 70 °C, and the patties were cooked sous-vide for 1 h at this temperature. After removing the cooked patties from the bags, they were directly grilled on a double-sided grill (Philips Health Grill, Philips, Amsterdam, The Netherlands) for 1 min at 200 °C.

### 2.3.2. pH and moisture content

The pH of the raw batter was measured, and the moisture content was determined by drying batter samples at 105 °C in an oven (Venticell, BMT Medical Technology, Brno, Czech Republic) for 24 h.

### 2.3.3. Rheological properties of patty batter

The rheological properties of the patty batter were measured with a stress-controlled rotational rheometer (MCR 302, Anton Paar, Graz, Austria) equipped with a plate-plate geometry (PP25/P2/SS – 78,336) with a diameter of 25 mm. Both plates had a profiled surface to prevent slip. To prepare the samples, 50 g of patty batter was transferred into a metal cylinder (diameter = 25 mm length = 80 mm) and compressed firmly to form a cylindrical sample. The samples were frozen for at least 12 h at  $-20$  °C and then sliced into 3 mm thick slabs using an electrical food slicer (Solida<sup>4</sup>, Ritterwerk GmbH, Gröbenzell, Germany). The slices were allowed to thaw, and were then placed on the bottom plate, after which the top plate was lowered until a normal force of 0.1 N was reached. Then the samples were compressed to 10% of their height and allowed to relax for 10 min. Subsequently, amplitude sweeps were performed at a strain ranging from 0.01 to 100%, at a constant frequency of 1 Hz and temperature of 20 °C. The storage modulus ( $G'$ ) was measured, from which the yield stress and yield strain were determined. Yield stress was defined as the value of the shear stress at the end of the linear viscoelastic regime (LVE), and was taken as the stress where  $G'$  deviated more than 5% from its strain-independent plateau value within the LVE. The yield strain was defined as the strain at the corresponding yield stress.

### 2.3.4. Cooking loss

The cooking loss (CL) was calculated as the mass loss of cooked patties during cooking as a percentage of the patty mass before cooking. This was done for the sous-vide cooking step to determine the sous-vide cooking loss,  $CL_{sv}$ , and the complete cooking process (sous-vide and grilling) to determine the total cooking loss,  $CL_{tot}$ , as:

$$CL_{sv} = \frac{m_{sv} - m_{raw}}{m_{raw}} \cdot 100\% \quad (6)$$

$$CL_{tot} = \frac{m_{tot} - m_{raw}}{m_{raw}} \cdot 100\% \quad (7)$$

where  $m_{sv}$  and  $m_{tot}$  are the masses of the patty after sous-vide cooking and grilling, respectively, and  $m_{raw}$  is the mass of the uncooked patty.

Additionally, the composition of the sous-vide cooking loss was analysed for oil, water and dry matter content. The released liquid was collected in a centrifuge tube and centrifuged at 1000 g for 1 min to separate the oil and the aqueous phase. The oil phase was decanted and weighed. The remaining aqueous phase was dried at 105 °C to determine dry matter and water content.

### 2.3.5. Textural properties and expressible liquid

Uniaxial compression tests were performed with a Texture Analyser (TA-XT plus, Stable Micro Systems Ltd., Godalming, UK) employed with a 50 kg load cell, to determine the textural properties of the patties, as well as their expressible liquid. Samples with a diameter of 30 mm and height of 20 mm were cut from the grilled patties using a cylindrical cutter and were allowed to cool down to an internal temperature of 70 °C. A stainless steel cylindrical probe with a diameter of 75 mm was used to compress the samples up to 80% strain with a speed of 1 mm/s, and a trigger force of 0.1 N. At the target position of 80% strain, the probe was held for 60 s to allow serum to be expelled, which was collected on a tissue paper placed underneath the samples. This tissue paper was weighed beforehand and directly after compression, giving information on the total expressible liquid (EL). After drying the tissues at 105 °C, the oil and water content of the EL were determined, allowing the quantification of the expressible water (EW) and oil (EO). EL, EW and EO were all expressed relative to the sample mass.

The Hencky strain ( $\epsilon = \ln L/L_0$ ) and stress ( $\sigma = F/A_t$ ) were also determined, where  $L$  is the height of the sample at any particular moment,  $L_0$  is the original height,  $F$  is the compression force and  $A_t$  is the time-dependent cross-sectional area of the sample. From the stress-strain curves, the Young's modulus ( $E$ ) was determined over the first 5% of deformation, and yield stress ( $\sigma_y$ ) and yield strain ( $\epsilon_y$ ) from the fracture point. All measurements were performed in duplicate.

### 2.4. Data analysis

All the commercial TVPs in this study had a different composition. To correct for these differences, measurements were also done on patties with ground TVP as a baseline for the contribution of the TVP material (composition) itself. The difference in WHC, cooking loss, expressible liquid and mechanical properties between intact and ground TVP samples is assumed to be related to the contribution of the structure to these parameters. The equations used to calculate these corrected values can be found in the supplementary information (Equation S1 – S8).

Unless stated otherwise, all results are presented as mean  $\pm$  standard error. Significant differences between samples were identified by a one-way analysis of variance (ANOVA), followed by a Dunnett's post-hoc test for all parameters reported in the study. A significance level of  $p < 0.05$  was used. Pearson correlation coefficients between TVP characteristics (structural features, protein content and bound water content), and functional properties of TVP and patties (water absorption and holding capacity, water absorption rate, rheological properties of the raw patty batter, cooking loss and its composition, expressible liquid, and textural properties of the grilled patties) were calculated based on their mean values. Data were analysed using the emmeans package (Lenth, 2023) with R (version 4.3.1) and Rstudio (version 2023.06.1 + 524).

### 3. Results & discussion

#### 3.1. Structural characterisation of TVPs

Detailed information on the structural characteristics of the various TVP samples was obtained using XRT. Fig. 1 visualises the microstructure of the thirteen TVPs obtained by XRT as two-dimensional image slices. Fig. 2 provides an example of the image analysis performed for one TVP (ROQ3) and Table 3 summarizes the results of the image analysis for all TVPs. Across the thirteen TVPs,  $\Phi_{XRT}$  ranged from 27.1 to 80.9%, MPS from 251 to 4790  $\mu\text{m}$ , MWT from 108 to 657  $\mu\text{m}$ , and  $\rho_{wall}$  from 597 to 1515  $\text{kg m}^{-3}$ , demonstrating that the TVPs differed substantially in numerous structural features. Additionally, Table 3 provides the values of apparent ( $\rho_{app}$ ) and absolute ( $\rho_{abs}$ ) density, protein content, and the bound water fraction of TVP chunks. The  $\rho_{app}$  ranged from 205 to 1042  $\text{kg m}^{-3}$  across TVPs, most likely because of different low-moisture extrusion conditions, resulting in different expansion ratios. In contrast, the  $\rho_{abs}$  varied within a narrow range between 1294 and 1389  $\text{kg m}^{-3}$ . This was expected, as  $\rho_{abs}$  represents the density of the powder without macroscopic pores, and therefore reflects the density of the material itself. The  $\Phi_{density}$  ranged from 22.8 to 81.4%, in agreement with values of  $\Phi_{XRT}$  ( $r = 0.85, p < 0.001$ ). The  $\Phi_{XRT}$  and  $\Phi_{density}$  deviated considerably from each other for some samples (ROQ3, ROQ4, GMI1, GMI2, and GMI3). In general, TVPs with  $\Phi_{XRT}$  lower than  $\Phi_{density}$  (ROQ3, ROQ4, ROQ5, GMI1, GMI2, GMI3, GMI4, and GMI6) had a relatively low wall density. This could be caused by the assumption made in XRT analysis that the TVP walls were completely solid. In reality, pores may be present within the walls on length scales smaller than the spatial resolution of the XRT, which was 15  $\mu\text{m}$ . Therefore, the pore volume may be underestimated in the XRT-method compared to the density-based method. Thus, both  $\Phi_{density}$  and  $\Phi_{XRT}$  give insight into the structure of the TVP, but  $\Phi_{density}$  includes nanopores within the walls, whereas

$\Phi_{XRT}$  identifies pores larger than 15  $\mu\text{m}$  only.

The protein content of the TVPs was found to range from 43.7 to 74.5%, pointing to large compositional differences between TVPs, besides the large differences in structural characteristics.

The bound water content of TVPs ranged between 12.5 and 21.8% and was positively correlated with protein content ( $r = 0.67, p < 0.05$ ). As protein is the main component in TVPs and has well-established water-binding properties, it was expected to play a predominant role in the binding of water in TVPs. The relatively large differences in bound water content between TVPs are likely to affect the release of water during cooking and compression. For a lower bound water content, more water is available to interact with other ingredients or to be released.

#### 3.2. Water absorption properties of TVP

The water absorption kinetics and maximum water absorption capacity (WAC) were investigated in rehydration experiments. Fig. 3 shows the water uptake as a function of time for all TVPs.

Water absorption depended strongly on TVP type, both in terms of kinetics of water uptake and maximum water uptake. Table 4 presents the results of fitting the experimental water absorption data to Equation (4) together with WAC determined in a separate experiment.

A significant and strong correlation ( $r = 0.96, p < 0.001$ ) between WAC and fit parameter  $a$  was observed, confirming that the parameter  $a$  represents the maximum amount of water the TVP can absorb. Nevertheless, the values for  $a$  were lower than the WAC values, most likely because the rehydration process was not completely finished yet after 20 min. To investigate how TVP structure influences the water uptake process, the structural characteristics of TVPs were correlated with the water absorption parameters (Table 5).

WAC correlated with  $\Phi_{XRT}$  ( $r = 0.61, p < 0.05$ ) and  $\Phi_{density}$  ( $r = 0.68, p < 0.05$ ), which supports our hypothesis that more water can be

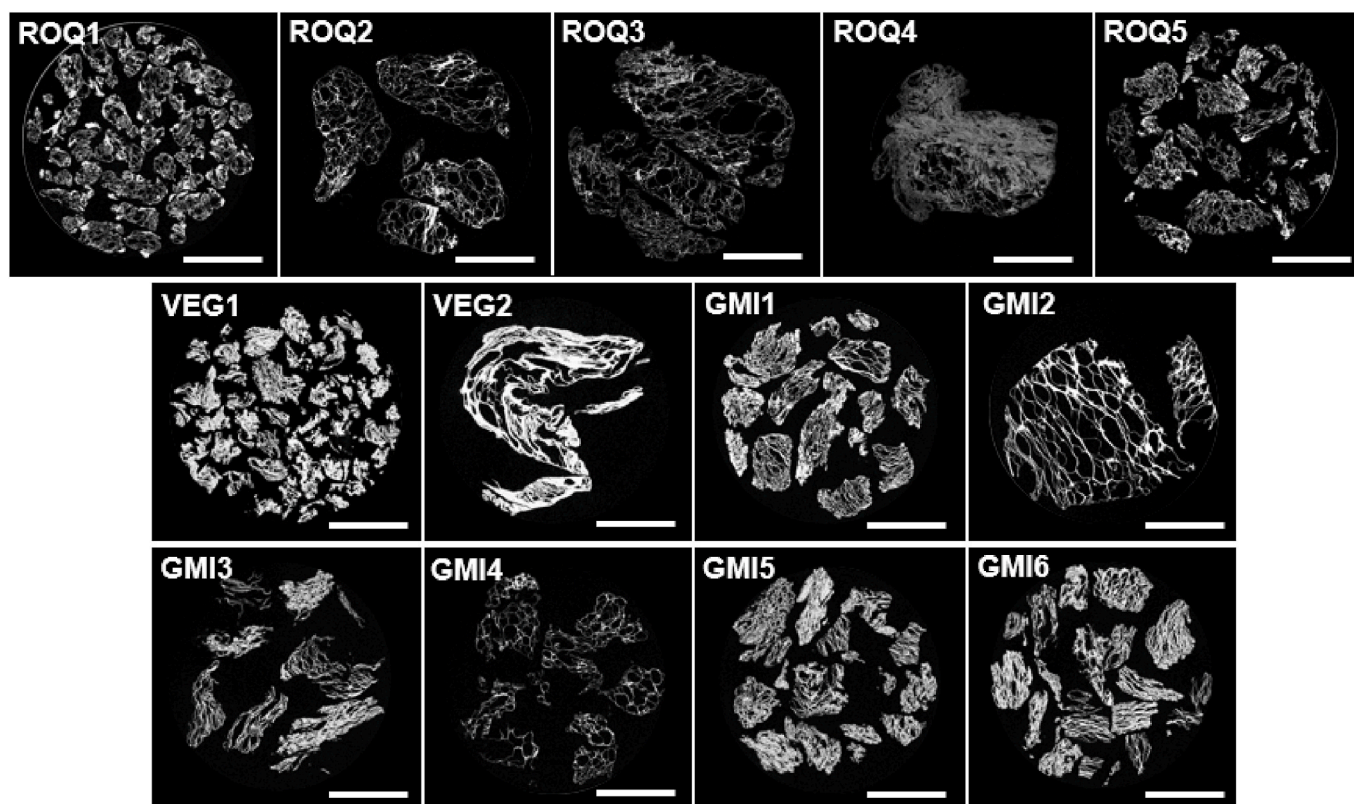
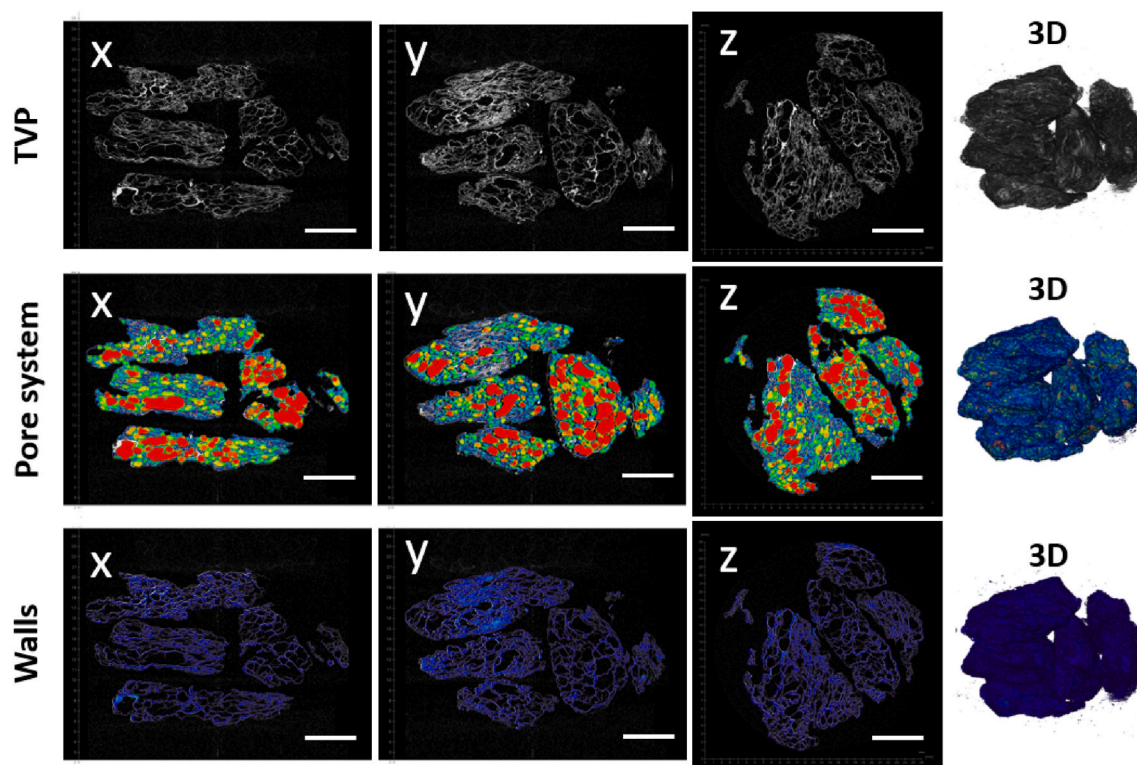


Fig. 1. Two-dimensional slices of X-ray microtomography images of all thirteen TVP chunks. The white scale bars represent 10 mm. Bright and black areas represent solid material and air, respectively.



**Fig. 2.** X-ray microtomography images of TVP chunks of ROQ3 and visualisation of pore size and wall thickness analysis. For simplicity, the analysis of 2D slices is shown here, while the analysis was performed on 3D stacks of 1500 images. In the top row, greyscale images of TVP are shown. In the second and third row, the thickness maps of the air phase and the wall phase inside TVP chunks is overlaid onto the greyscale images from the top row. All rows consist of two-dimensional image slices in an example x, y and z plane, followed by the reconstructed trimetric image. For simplicity, the colour bar with size distributions was removed. The white scale bars represent 5 mm.

absorbed by TVPs with higher porosity. The slightly higher correlation coefficient for  $\Phi_{\text{density}}$  ( $r = 0.68$ ) than  $\Phi_{\text{XRT}}$  ( $r = 0.61$ ) might suggest that the nanopores, included in  $\Phi_{\text{density}}$ , were relevant for water absorption. The relationship between porosity and WAC has been suggested in previous studies on textured protein (Hong et al., 2022; Ning & Villota, 1994; Samard & Ryu, 2019b), but has only been experimentally demonstrated by Lee et al. (J.-S. Lee et al., 2022). Our results confirm this relationship across a broad range of commercially available TVPs.

A negative correlation between WAC and MWT ( $r = -0.63$ ,  $p < 0.05$ ) was found, suggesting that TVPs with thinner walls absorbed more water. However, TVPs with higher porosity also tended to have thinner walls. MWT was the only parameter correlated with  $b_1$  ( $r = 0.66$ ,  $p < 0.05$ ), suggesting that MWT is the main factor determining initial uptake rate. This correlation indicates that thicker walls resulted in faster initial water uptake, while thinner walls were found to be more favourable for a higher maximum WAC (Table 5). Since thicker walls embody a larger volume of material than thinner walls, more water can flow through them in the initial stages of water absorption. In later stages, water absorption in TVPs with thicker walls becomes limited, as there is less pore space for the TVP walls to swell into as they absorb water.

Parameter  $b_2$ , which captures prolonged water uptake at longer timescales, did not significantly correlate with any structural characteristic. Among all the structural characteristics, MPS had the highest correlation ( $r = 0.47$ ) with  $b_2$ , though not significant. The slow component of an absorption process is usually related to the relaxation of the structure, while the fast component is due to intrinsic water holding capacity and capillarity. Therefore, we presume the weak correlation between MPS and  $b_2$  may be related to the deformability of the walls and the shape and size of the pores present in TVP. Larger pores may allow more wall deformation, and thus faster swelling.

Fit parameter  $b_1$  was generally one to two or three orders of

magnitude larger than  $b_2$ . One to three orders of magnitude differences between  $b_1$  and  $b_2$  have been previously reported for various materials including fibres and textile products (Hamdaoui et al., 2014; Kohler et al., 2003; Okubayashi et al., 2004, 2005; Zou et al., 2022). These differences imply that the initial water uptake by TVPs happens much faster than the water uptake at longer time scales. Hodge et al. (Hodge et al., 1996) showed that initial water uptake by PVA films was mainly attributed to bound water. For later stages, they found that the free water content increased. Kachrimanis et al. (Kachrimanis et al., 2006) suggested a similar mechanism for the water absorption process of microcrystalline cellulose. In our study, no correlations were found between bound water content of TVPs and water absorption kinetics. This can probably be attributed to the different nature of our samples compared to PVA films and microcrystalline cellulose.

To summarize, water absorption by TVPs consists of a fast, initial absorption process during which thick TVP walls promote the uptake of water and a slow, late absorption process during which thin TVP walls and high porosity promote maximum water absorption capacity.

### 3.2.1. XRT visualisation of water absorption by TVPs

To gain insights into the mechanisms behind water absorption, the effect of the rehydration process of TVPs on its structure was visualised using XRT. Fig. 4 shows a sequence of images of the microstructure of one TVP type (ROQ2) at various water absorption stages.

The image sequence illustrates the swelling of TVP walls as water is absorbed, leading to the expansion of the TVP chunks during rehydration. The highest absorbed water content (300%) of TVP (ROQ2) in Fig. 4 was slightly below the maximum WAC of 336% (Table 4). At a water content of 300%, the TVP walls were considerably thicker than at lower water content, while pores were still visible. It is likely that at the maximum WAC (336%), slightly less pores would be present. As XRT cannot distinguish well between water and air, the presence of water in

**Table 3** Characteristics of thirteen TVPs: XRT-based porosity ( $\phi_{XRT}$ ), mean pore size (MPS), mean wall thickness (MWT), wall density ( $\rho_{wall}$ ) as obtained from XRT measurements; apparent density ( $\rho_{app}$ ), absolute density ( $\rho_{abs}$ ) and density-based porosity ( $\phi_{density}$ ) from density measurements; protein content as obtained from the Dumas method; bound water content derived from DSC measurements. Means are reported with standard error. Means sharing superscript letters are not significantly different ( $p > 0.05$ ). Significance for bound water content was not determined, as this was obtained from data regression.

TVP type	XRT				Density measurements			Dumas		DSC	
	$\phi_{XRT}$ (%)	MPS ( $\mu m$ )	MWT ( $\mu m$ )	$\rho_{wall}$ ( $kg \cdot m^{-3}$ )	$\rho_{app}$ ( $kg \cdot m^{-3}$ )	$\rho_{abs}$ ( $kg \cdot m^{-3}$ )	$\phi_{density}$ (%)	Protein content (w/w %)	Bound water content (w/w %)		
ROQ1	63.8 ± 6.7 <sup>cd</sup>	526 ± 79 <sup>ab</sup>	239 ± 3 <sup>abc</sup>	1379 ± 267 <sup>c</sup>	500 ± 30 <sup>def</sup>	1303 ± 3 <sup>b</sup>	60.3 ± 2.3 <sup>bcd</sup>	68.8 ± 0.1 <sup>e</sup>	16.5 ± 4.2		
ROQ2	80.9 ± 1.1 <sup>d</sup>	1921 ± 382 <sup>c</sup>	196 ± 37 <sup>ab</sup>	1298 ± 80 <sup>abc</sup>	248 ± 5 <sup>a</sup>	1298 ± 1 <sup>b</sup>	78.0 ± 0.6 <sup>ef</sup>	68.9 ± 0.1 <sup>e</sup>	19.4 ± 1.5		
ROQ3	65.7 ± 12.0 <sup>cd</sup>	3152 ± 655 <sup>bc</sup>	108 ± 5 <sup>b</sup>	597 ± 209 <sup>a</sup>	205 ± 5 <sup>a</sup>	1294 ± 3 <sup>b</sup>	81.4 ± 0.5 <sup>f</sup>	69.4 ± 0.1 <sup>e</sup>	19.9 ± 1.7		
ROQ4	44.1 ± 7.2 <sup>abc</sup>	1663 ± 665 <sup>abc</sup>	480 ± 65 <sup>e</sup>	647 ± 86 <sup>ab</sup>	362 ± 10 <sup>bcd</sup>	1342 ± 3 <sup>c</sup>	69.6 ± 1.4 <sup>def</sup>	60.4 ± 0.2 <sup>c</sup>	15.4 ± 2.2		
ROQ5	57.7 ± 1.7 <sup>bcd</sup>	559 ± 44 <sup>ab</sup>	266 ± 15 <sup>abc</sup>	1036 ± 107 <sup>abc</sup>	438 ± 42 <sup>bcd</sup>	1307 ± 5 <sup>b</sup>	65.8 ± 3.3 <sup>bcd</sup>	63.8 ± 0.1 <sup>d</sup>	17.9 ± 1.4		
VEG1	27.1 ± 0.8 <sup>a</sup>	251 ± 149 <sup>a</sup>	287 ± 4 <sup>de</sup>	1429 ± 92 <sup>c</sup>	1042 ± 66 <sup>g</sup>	1364 ± 2 <sup>d</sup>	22.8 ± 4.9 <sup>a</sup>	63.5 ± 0.8 <sup>d</sup>	21.8 ± 1.4		
VEG2	32.0 ± 2.7 <sup>a</sup>	2817 ± 363 <sup>d</sup>	657 ± 60 <sup>f</sup>	1515 ± 65 <sup>c</sup>	1031 ± 17 <sup>g</sup>	1375 ± 2 <sup>d</sup>	24.0 ± 1.3 <sup>a</sup>	43.7 ± 1.7 <sup>a</sup>	12.5 ± 1.9		
GMI1	39.8 ± 1.7 <sup>ab</sup>	554 ± 48 <sup>ab</sup>	219 ± 9 <sup>abcd</sup>	973 ± 53 <sup>bc</sup>	586 ± 27 <sup>ef</sup>	1406 ± 6 <sup>c</sup>	58.4 ± 2.0 <sup>bc</sup>	50.1 ± 0.2 <sup>b</sup>	14.5 ± 1.5		
GMI2	64.9 ± 1.0 <sup>cd</sup>	4790 ± 996 <sup>d</sup>	220 ± 3 <sup>abcd</sup>	888 ± 116 <sup>abc</sup>	312 ± 40 <sup>abc</sup>	1380 ± 1 <sup>d</sup>	77.9 ± 2.8 <sup>ef</sup>	47.9 ± 0.2 <sup>ab</sup>	13.6 ± 2.2		
GMI3	48.1 ± 2.1 <sup>abc</sup>	274 ± 28 <sup>ab</sup>	216 ± 7 <sup>abcd</sup>	957 ± 117 <sup>abc</sup>	497 ± 57 <sup>def</sup>	1338 ± 1 <sup>c</sup>	63.8 ± 4.2 <sup>bcd</sup>	70.5 ± 0.1 <sup>e</sup>	17.3 ± 2.7		
GMI4	74.4 ± 0.8 <sup>d</sup>	1975 ± 526 <sup>e</sup>	152 ± 8 <sup>ab</sup>	1198 ± 38 <sup>bc</sup>	307 ± 3 <sup>ab</sup>	1273 ± 2 <sup>a</sup>	74.4 ± 0.3 <sup>def</sup>	74.5 ± 0.1 <sup>f</sup>	17.0 ± 3.1		
GMI5	36.5 ± 2.5 <sup>ab</sup>	536 ± 76 <sup>ab</sup>	319 ± 19 <sup>cde</sup>	1413 ± 116 <sup>c</sup>	898 ± 65 <sup>g</sup>	1306 ± 2 <sup>b</sup>	30.3 ± 5.1 <sup>a</sup>	69.2 ± 0.3 <sup>c</sup>	16.8 ± 3.1		
GMI6	42.2 ± 3.2 <sup>abc</sup>	372 ± 86 <sup>ab</sup>	248 ± 9 <sup>bcd</sup>	1089 ± 62 <sup>abc</sup>	629 ± 8 <sup>f</sup>	1302 ± 0 <sup>b</sup>	50.8 ± 0.7 <sup>b</sup>	74.2 ± 0.1 <sup>f</sup>	17.2 ± 1.1		

the pores could not be verified. It is hypothesised that the pores present in ROQ2 (300%, Fig. 4) probably contained water, which should be more prevalent for small pores than large ones, due to larger capillary forces on water in small pores.

### 3.2.2. Discussion of water absorption mechanism

Based on the findings discussed above, we hypothesised that mainly capillary forces, induced by the nanoscale pores within the walls of TVPs, drive the absorption of water into the walls. In the early stages of water absorption, thicker walls were found to promote the absorption of larger volumes of water. This is reminiscent of Jurin's law, which shows that the volume of water absorbed by a capillary is proportional to its radius (de Gennes et al., 2004). However, Jurin's law assumes idealised cylindrical capillaries, whereas the TVP walls contain solid material and an intricate system of nanochannels. The capillary forces in TVP responsible for water uptake most likely act within the walls of TVPs, as pore size and water absorption properties were not correlated. On the other hand, at longer time scales, thinner walls increased the maximum WAC. TVPs with thinner walls usually have higher porosity, potentially resulting in more space for wall swelling, and thus allowing more water to be absorbed. Eventually, water absorption probably leads to a self-sealing effect (Rucker-Gramm & Beddoe, 2010; Tang et al., 2008), in which the connectivity of the pore system is reduced and further water uptake is slowed down. In TVPs, the reduction of connectivity likely takes place within the walls, where the nanopores as well as the hydrophilic material are filled as water is absorbed. Even at the maximum WAC, macroscopic pores are still present in TVP, which can hold water depending on their size. Smaller pores are likely to hold water more easily due to larger capillary forces compared to larger pores. For TVPs with thin walls, we speculate based on Fig. 4, that the contribution of water held in pores to the total WAC is limited compared to the contribution of water absorbed by the walls. The contribution of the pores to the WAC likely becomes larger for TVP with thicker walls, as less water can be held in the walls and the total WAC of these TVPs is lower.

Besides the role of capillary action within the walls and in the pores, also the TVP material, which mainly consists of protein, absorbs substantial amounts of water in the absence of a porous structure. Different TVPs may have differences in number of exposed water-binding sites as influenced by the protein type or degree of protein unfolding, and presence of fibres, starches and polysaccharides with different water absorption properties. However, we expect that the contribution of the composition of TVP will be relatively similar for all TVPs, as previously shown by Hong et al. (Hong et al., 2022). These researchers measured the WAC of 28 commercial TVPs and found that ground pea, soy and wheat-based TVPs absorbed similar amounts of water (210, 210 and 190% water, expressed as a percentage of the dry mass of the TVP) despite large differences in protein content between TVPs (pea 72.7 wt %, soy 51.4 wt% and wheat 68.3 wt%).

During water absorption, the pore network is not completely filled up by the swelling walls (Fig. 4), suggesting that the flexibility and expandability of the walls may be a factor limiting water absorption. According to standard beam theory and the Gibson–Ashby model derived from this theory (Agbisit et al., 2007; Gibson & Ashby, 1997), increasing beam thickness and decreasing beam length lead to higher stiffness and failure strength. Therefore, thinner and longer walls of TVPs are more deformable than thicker and shorter walls. The length of a wall is defined as the distance between the junction zones of the walls, which is larger when the pores are larger. As a measure for wall deformability, we calculated the ratio of MPS to MWT for all TVPs, which includes the information of wall length and wall thickness. It was found that this ratio correlated well with the WAC ( $r = 0.75$ ,  $p < 0.01$ ), indicating the importance of the deformability of walls in WAC.

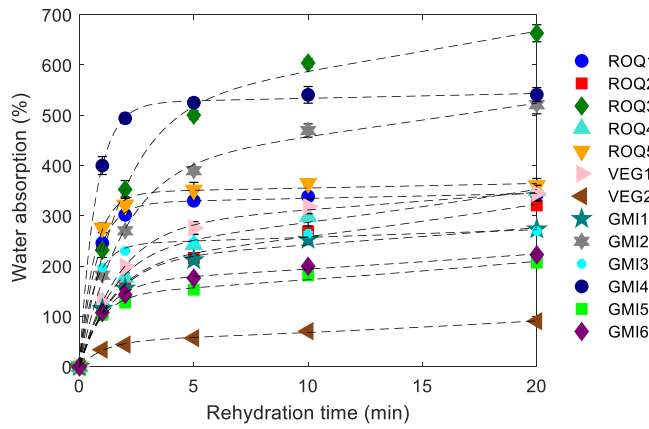


**Fig. 3.** Water absorption over time for different TVP types. The dotted lines represent the best fit for  $w = a(e^{b_1 t} - e^{b_2 t})$ , where  $w$  is the absorbed water,  $a$  is the maximum amount of water that can be absorbed,  $b_1$  and  $b_2$  are two rate constants and  $t$  is time.

**3.3. Water holding properties of TVP**

The water holding properties of TVP are related to the release of water when an external force is applied to the TVP. Table 6 presents the water holding capacity (WHC) of intact ( $WHC_{intact}$ ) and ground ( $WHC_{ground}$ ) TVPs, and the difference between  $WHC_{intact}$  and  $WHC_{ground}$ , shown as  $WHC_{structure}$ .

$WHC_{intact}$  and  $WHC_{ground}$  showed large variations, with values ranging from 77.1% to 364.4% and 96.9% and 321.6%, respectively. This suggests that both the structure of the TVPs and the TVP-material itself have a strong impact on the water holding capacity. Nine out of thirteen TVPs had a positive  $WHC_{structure}$ , indicating that intact TVP chunks held more water than the ground TVP material itself. Interestingly, four TVPs (ROQ4, ROQ5, GMI1 and GMI5) had a negative  $WHC_{structure}$ , implying that the structure of TVP negatively influenced the WHC of the material itself. This may be due to a larger surface area of the ground TVP compared to intact TVP, thereby providing more binding sites for water molecules, promoting a higher WHC. This effect could be different for each TVP because of the differences in composition and processing conditions. Additionally, very dense parts of TVPs that prevent water from being absorbed could be opened up during the grinding of TVP chunks. Table 7 reports the correlation coefficients between the water holding properties and the structural characteristics of TVPs.

$WHC_{intact}$  was positively correlated with both  $\Phi_{XRT}$  ( $r = 0.78, p < 0.01$ ) and  $\Phi_{density}$  ( $r = 0.73, p < 0.01$ ). This indicates that the higher the porosity of TVPs, the more water can be held in TVPs during centrifugation. This correlation was similar for WAC, for which a higher porosity

**Table 4**

Water absorption capacity (WAC) and fit parameters  $a$ ,  $b_1$  and  $b_2$  obtained from the best fit through the data of water absorption for all TVPs. Means are reported with standard error. Means sharing superscript letters are not significantly different ( $p > 0.05$ ).

TVP type	VP type	WAC (%)	a (%)	$b_1$ (s <sup>-1</sup> )	$b_2$ (s <sup>-1</sup> )
ROQ1		397 ± 4 <sup>e</sup>	325 ± 0 <sup>fg</sup>	0.003 ± 0.000 <sup>ab</sup>	-1.372 ± 0.027 <sup>ab</sup>
ROQ2		336 ± 3 <sup>cd</sup>	207 ± 9 <sup>cd</sup>	0.022 ± 0.001 <sup>fg</sup>	-0.694 ± 0.001 <sup>cd</sup>
ROQ3		709 ± 5 <sup>b</sup>	523 ± 2 <sup>i</sup>	0.012 ± 0.001 <sup>bcd</sup>	-0.531 ± 0.059 <sup>d</sup>
ROQ4		382 ± 16 <sup>de</sup>	234 ± 21 <sup>de</sup>	0.021 ± 0.002 <sup>efg</sup>	-0.679 ± 0.043 <sup>d</sup>
ROQ5		488 ± 12 <sup>f</sup>	347 ± 13 <sup>g</sup>	0.003 ± 0.000 <sup>ab</sup>	-1.521 ± 0.014 <sup>ab</sup>
VEG1		401 ± 1 <sup>e</sup>	282 ± 13 <sup>ef</sup>	0.010 ± 0.000 <sup>abcd</sup>	-0.586 ± 0.007 <sup>d</sup>
VEG2		134 ± 4 <sup>a</sup>	51 ± 7 <sup>a</sup>	0.030 ± 0.005 <sup>g</sup>	-0.935 ± 0.058 <sup>cd</sup>
GMI1		298 ± 20 <sup>c</sup>	213 ± 5 <sup>cd</sup>	0.013 ± 0.002 <sup>cdef</sup>	-0.664 ± 0.020 <sup>d</sup>
GMI2		533 ± 2 <sup>fg</sup>	403 ± 7 <sup>h</sup>	0.013 ± 0.001 <sup>cdef</sup>	-0.531 ± 0.007 <sup>d</sup>
GMI3		339 ± 7 <sup>cd</sup>	243 ± 3 <sup>de</sup>	0.006 ± 0.000 <sup>abc</sup>	-1.601 ± 0.116 <sup>a</sup>
GMI4		552 ± 6 <sup>g</sup>	526 ± 8 <sup>i</sup>	0.002 ± 0.001 <sup>a</sup>	-1.442 ± 0.216 <sup>ab</sup>
GMI5		235 ± 2 <sup>b</sup>	143 ± 5 <sup>b</sup>	0.019 ± 0.000 <sup>def</sup>	-1.124 ± 0.014 <sup>bc</sup>
GMI6		223 ± 5 <sup>b</sup>	168 ± 4 <sup>bc</sup>	0.014 ± 0.001 <sup>cdef</sup>	-0.938 ± 0.076 <sup>cd</sup>

**Table 5**

Pearson correlation coefficients ( $r$ ) between water absorption capacity (WAC) and fit parameters  $a$ ,  $b_1$  and  $b_2$  and XRT-based porosity ( $\Phi_{XRT}$ ), mean pore size (MPS), mean wall thickness (MWT), TVP density ( $\rho_{TVP}$ ), wall density ( $\rho_{wall}$ ) density-based porosity ( $\Phi_{density}$ ).

	$\Phi_{XRT}$	MPS	MWT	$\rho_{wall}$	$\rho_{app}$	$\Phi_{density}$
WAC	<b>0.61*</b>	0.42	-0.63*	-0.57*	-0.68*	<b>0.68*</b>
a	<b>0.64*</b>	0.35	-0.69**	-0.46	-0.66*	<b>0.66*</b>
$b_1$	-0.34	0.32	<b>0.66*</b>	0.15	0.34	-0.35
$b_2$	-0.13	0.47	0.07	-0.26	0.00	0.01

\* = significance at  $p < 0.05$ , \*\* = significance at  $p < 0.001$ .

was related to higher swelling capacity and subsequent higher water absorption. This is confirmed by the positive correlation between  $WHC_{intact}$  and WAC ( $r = 0.84, p < 0.001$ ). Logically,  $WHC_{ground}$  did not correlate with any of the structural characteristics, as ground TVP lacked such features. However, the differences in  $WHC_{ground}$  for the TVPs suggest a significant influence of composition. In the current study, we only measured the protein content of the samples, which did not correlate with the  $WHC_{ground}$ . Hence, the origin of the differences between TVPs in  $WHC_{ground}$  remains unclear.

$WHC_{structure}$  correlated only with  $\Phi_{XRT}$  ( $r = 0.56, p < 0.05$ ), supporting the hypothesis provided for  $WHC_{intact}$  that the pore system in TVPs is of major importance for water holding capacity. Stronger correlations were anticipated between the  $WHC_{structure}$  and other structural properties, given that this WHC-value has been corrected for the intrinsic water holding properties of the TVP material. As WAC was related to wall properties, a correlation between wall properties and WHC was also expected. However, no significant correlations were observed. In spite of this, when  $WHC_{structure}$  was plotted as function of MWT (Fig. 5), a trend was visible for eleven out of thirteen samples, confirming our expectation that these parameters should be related. The trend was weakened by two outliers (ROQ4 and VEG2). After excluding the outliers, the correlation coefficient between  $WHC_{structure}$  and MWT increased to  $r = -0.72$  and became significant ( $p < 0.05$ ). To explain why ROQ4 and VEG2 are outliers, the microstructure of these TVPs is shown in Fig. 5.

ROQ4 and VEG2 had different structural characteristics compared to the other TVPs. ROQ4 (denoted by image A in Fig. 5) was the only TVP made from fava bean and was found to have a highly heterogenous structure, with some parts of the TVP chunks being extremely dense and others containing numerous large pores. This heterogeneity complicated the determination of a mean pore radius and wall thickness, resulting in a large variance in these parameters for this sample (supplementary information, Table S3). The heterogeneity of the internal structure is known to impact functional properties of low-moisture extruded material (Guillermic et al., 2021), which could explain the low correlation between  $WHC_{structure}$  and MWT for this TVP. The soy-based VEG2

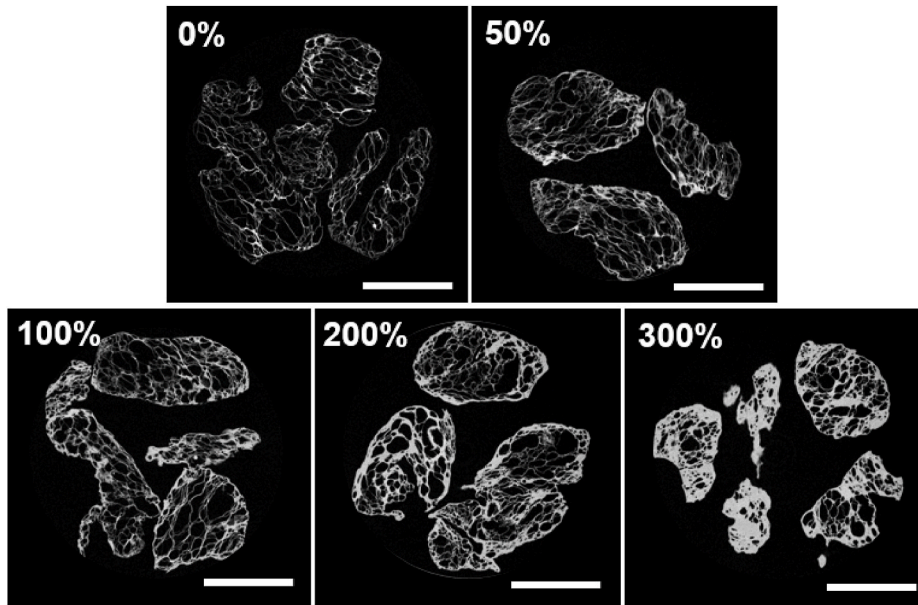


Fig. 4. Two-dimensional X-ray microtomography images of ROQ2 differing in absorbed water content, given as a percentage of the dry mass of the TVP. The white scale bars represent 10 mm.

(denoted by image B in Fig. 5) had the thickest and densest walls among all TVPs (Table 3). It had the lowest protein content, lowest bound water content and relatively few surface openings compared to other TVPs. This may partially explain the low WAC of VEG2 (Fig. 3), as water could not easily enter the TVP.

In conclusion, structural characteristics of TVPs influenced the water absorption and water holding properties. Particularly, higher porosity and thinner walls improved water absorption and holding capacity. As water absorption and water holding behaviour of TVP are suggested to play a large role in the properties of meat analogues, the relation between the structural characteristics of TVP and different characteristics of plant-based patties was evaluated.

### 3.4. Functional properties of batter and patties

#### 3.4.1. Rheological properties of patty batter

The rheological properties of patty batter are important for batter handleability and processability during various stages of production. To investigate the effect of TVP on the rheological properties of the raw patty batter, yield stress and yield strain were determined and are presented in Table 8.

For patty batters with intact TVPs, the yield stress and yield strain

Table 6

Water holding capacity (WHC) for intact (WHC<sub>intact</sub>) and ground (WHC<sub>ground</sub>) TVPs, and WHC<sub>structure</sub>. Means are reported with standard error. Means sharing superscript letters are not significantly different ( $p > 0.05$ ).

TVP type	WHC <sub>intact</sub> (%)	WHC <sub>ground</sub> (%)	WHC <sub>structure</sub> (-)
ROQ1	207.4 ± 7.8 <sup>de</sup>	168.4 ± 9.0 <sup>cde</sup>	38.9 ± 11.9 <sup>cdef</sup>
ROQ2	245.7 ± 6.7 <sup>f</sup>	182.7 ± 8.9 <sup>de</sup>	63.0 ± 11.1 <sup>def</sup>
ROQ3	364.4 ± 14.1 <sup>g</sup>	279.2 ± 19.2 <sup>f</sup>	85.1 ± 23.8 <sup>ef</sup>
ROQ4	188.0 ± 5.5 <sup>cd</sup>	217.1 ± 17.8 <sup>c</sup>	-29.1 ± 18.6 <sup>bc</sup>
ROQ5	201.5 ± 2.9 <sup>de</sup>	321.6 ± 8.9 <sup>f</sup>	-120.1 ± 9.4 <sup>a</sup>
VEG1	161.1 ± 0.6 <sup>bc</sup>	150.9 ± 7.4 <sup>abcd</sup>	10.2 ± 7.4 <sup>cde</sup>
VEG2	106.1 ± 3.8 <sup>a</sup>	96.9 ± 0.2 <sup>a</sup>	9.1 ± 3.8 <sup>cde</sup>
GMI1	154.1 ± 1.9 <sup>bc</sup>	157.1 ± 15.5 <sup>bcd</sup>	-3.0 ± 15.6 <sup>bcd</sup>
GMI2	236.6 ± 10.2 <sup>ef</sup>	129.1 ± 4.4 <sup>abcd</sup>	107.4 ± 11.1 <sup>f</sup>
GMI3	163.2 ± 1.9 <sup>bc</sup>	112.5 ± 0.5 <sup>ab</sup>	50.6 ± 1.9 <sup>cdef</sup>
GMI4	408.7 ± 0.0 <sup>h</sup>	146.6 ± 0.5 <sup>abcd</sup>	262.2 ± 0.5 <sup>g</sup>
GMI5	77.1 ± 6.0 <sup>a</sup>	161.7 ± 0.9 <sup>bcd</sup>	-84.6 ± 6.1 <sup>ab</sup>
GMI6	145.2 ± 7.1 <sup>b</sup>	117.9 ± 1.3 <sup>abc</sup>	27.2 ± 7.3 <sup>cdef</sup>

ranged from 12.9 to 35.2 kPa and 0.12–0.29%, respectively. The yield stress and yield strain of patty batters with ground TVPs varied from 9.1 to 22.0 kPa and 0.13–0.36%, respectively. Since ten out of thirteen batters have a higher yield strain for the ground product, the presence of TVP structure clearly resulted in batters that started to flow at higher yield stresses but at lower yield strains. This finding suggests that patty batters were stronger but less deformable. The correlations between all physicochemical properties of patty batters including the rheological properties and the structural characteristics of the TVPs can be found in the Appendix (Table A1 and A2). The most important correlations are discussed here below.

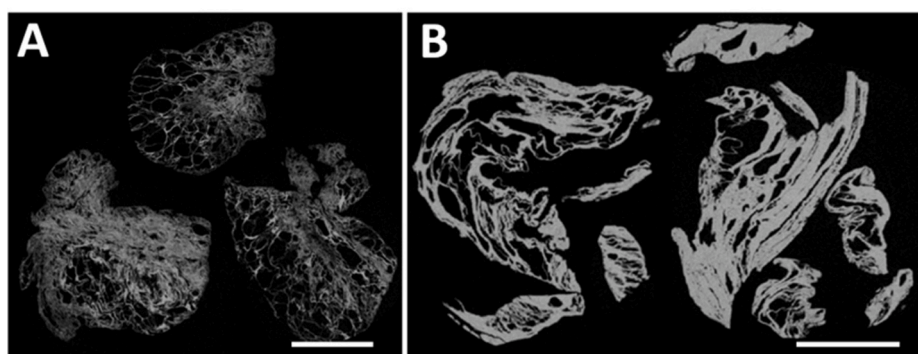
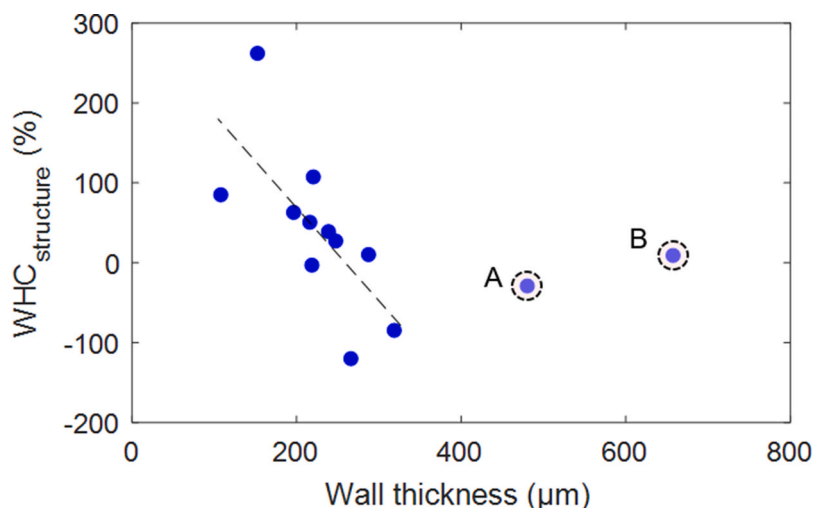
A significant correlation was found between MWT and yield stress that was corrected for the contribution of the TVP composition ( $\sigma_{y-structure}$ ,  $r = 0.70$ ,  $p < 0.01$ , Appendix, Table A2) as calculated according to Equation S5. This correction was done by looking at the ratio of  $\sigma_y$  for patties with intact TVP and ground TVP, to exclude the effect of the differences in composition between TVPs. The significant correlation suggests that the wall network within TVPs was the main contributor to the elastic properties of the patty batter. This finding implies that thicker walls allow for more energy to be stored elastically in the patty batter. As samples with low MWT tended to have a higher porosity, it could be that TVP with thicker walls had a higher overall wall volume, meaning more material was available to store energy. These results are consistent with previous studies (Agbisit et al., 2007; Barrett & Peleg, 1992; Ganesan et al., 2019; Yang et al., 2022), which reported increased strength for porous materials with thicker walls. Not only the wall thickness itself, but also the variance in MWT ( $\sigma_{MWT}^2$ ), as a measure of the heterogeneous nature of the walls, positively correlated with  $\sigma_{y-structure}$  ( $r = 0.80$ ,  $p <$

Table 7

Pearson correlation coefficients ( $r$ ) between the XRT-based porosity ( $\Phi_{XRT}$ ), mean pore size (MPS), mean wall thickness (MWT), wall density ( $\rho_{wall}$ ), TVP density ( $\rho_{wall}$ ) and density-based porosity ( $\Phi_{density}$ ) and water holding properties of TVP.

	$\Phi_{XRT}$	MPS	MWT	$\rho_{wall}$	$\rho_{app}$	$\Phi_{density}$
WHC <sub>intact</sub>	<b>0.78**</b>	0.44	-0.59	-0.40	<b>-0.74**</b>	<b>0.73**</b>
WHC <sub>ground</sub>	0.32	-0.01	-0.25	-0.46	-0.45	0.42
WHC <sub>structure</sub>	<b>0.56*</b>	0.45	-0.42	-0.08	-0.43	0.44

\* = significance at  $p < 0.05$ , \*\* = significance at  $p < 0.01$ .



**Fig. 5.**  $WHC_{structure}$  as function of wall thickness for all TVPs. Dashed line shows the main trend in the data set. Outliers A and B are visualised in the form of two-dimensional XRT-images depicting TVPs ROQ4 and VEG2, respectively. The white scale bars represent 1 cm in both images.

**Table 8**

Yield stress ( $\sigma_y$ ) and yield strain ( $\epsilon_y$ ) of patty batter made with intact and ground TVP. Means are reported with standard error. Means sharing superscript letters are not significantly different ( $p > 0.05$ ).

TVP type	Patty batter made with intact TVP		Patty batter made with ground TVP	
	$\sigma_y$ (kPa)	$\epsilon_y$ (%)	$\sigma_y$ (kPa)	$\epsilon_y$ (%)
ROQ1	24.8 ± 1.0 <sup>de</sup>	0.17 ± 0.02 <sup>a</sup>	17.8 ± 0.8 <sup>cde</sup>	0.25 ± 0.00 <sup>abc</sup>
ROQ2	33.0 ± 3.0 <sup>ef</sup>	0.13 ± 0.02 <sup>a</sup>	18.6 ± 1.3 <sup>de</sup>	0.23 ± 0.05 <sup>abc</sup>
ROQ3	35.2 ± 1.0 <sup>f</sup>	0.15 ± 0.03 <sup>a</sup>	21.0 ± 1.1 <sup>de</sup>	0.25 ± 0.00 <sup>abc</sup>
ROQ4	30.4 ± 2.1 <sup>def</sup>	0.22 ± 0.01 <sup>ab</sup>	20.7 ± 1.3 <sup>de</sup>	0.26 ± 0.02 <sup>abc</sup>
ROQ5	25.7 ± 2.0 <sup>de</sup>	0.12 ± 0.01 <sup>a</sup>	17.8 ± 0.3 <sup>cde</sup>	0.34 ± 0.02 <sup>c</sup>
VEG1	26.0 ± 0.9 <sup>de</sup>	0.13 ± 0.01 <sup>a</sup>	22.0 ± 1.2 <sup>e</sup>	0.13 ± 0.01 <sup>a</sup>
VEG2	33.5 ± 1.1 <sup>ef</sup>	0.14 ± 0.02 <sup>a</sup>	9.1 ± 0.3 <sup>a</sup>	0.26 ± 0.02 <sup>abc</sup>
GMI1	22.0 ± 2.5 <sup>bcd</sup>	0.17 ± 0.02 <sup>a</sup>	20.2 ± 0.6 <sup>de</sup>	0.24 ± 0.04 <sup>abc</sup>
GMI2	23.3 ± 1.2 <sup>cd</sup>	0.19 ± 0.01 <sup>ab</sup>	17.7 ± 0.3 <sup>cd</sup>	0.14 ± 0.02 <sup>a</sup>
GMI3	14.3 ± 1.0 <sup>ab</sup>	0.22 ± 0.01 <sup>ab</sup>	13.8 ± 0.4 <sup>bc</sup>	0.28 ± 0.02 <sup>bc</sup>
GMI4	28.6 ± 2.7 <sup>def</sup>	0.16 ± 0.02 <sup>a</sup>	19.8 ± 1.0 <sup>de</sup>	0.18 ± 0.04 <sup>ab</sup>
GMI5	12.9 ± 0.7 <sup>a</sup>	0.29 ± 0.04 <sup>b</sup>	12.4 ± 0.5 <sup>ab</sup>	0.36 ± 0.00 <sup>c</sup>
GMI6	14.7 ± 0.9 <sup>abc</sup>	0.22 ± 0.03 <sup>ab</sup>	11.9 ± 0.3 <sup>ab</sup>	0.29 ± 0.04 <sup>bc</sup>

0.01, Appendix, Table A2). The importance of wall thickness homogeneity has been emphasised previously by other studies (Agbisit et al., 2007; Guillermic et al., 2021), as a more uniform wall thickness mitigates stress concentration. Consequently, it deters the formation of regions where material failure is more likely, ultimately resulting in a stronger material. It is important to note that these studies focused on dry extrudates, and the behaviour of these extrudates may be different after rehydration and incorporation into a patty batter. In our study, both the mean wall thickness of TVP and its variance were correlated to yield stress of patty batters. Therefore, it remains unclear which of the

two is most important here.

### 3.4.2. Cooking loss

For both the patties with intact and ground TVP, the cooking loss (CL) during preparation was determined. Table 9 presents the sous-vide CL, total CL (sous-vide + grilling loss) and the composition of the sous-vide CL of all cooked patties.

Patties prepared with different types of intact TVPs showed significant differences in both sous-vide CL and total CL. Grinding resulted in a decreased sous-vide CL for six TVPs (ROQ1, ROQ2, ROQ3, ROQ4, ROQ5 and VEG1), while the other seven TVPs (VEG2, GMI1, GMI2, GMI3, GMI4, GMI5, GMI6) showed an increased sous-vide CL. Strikingly, five of the six TVPs with a decreased sous-vide CL when ground, were produced by Roquette, and six of the seven TVPs that showed an increased sous-vide CL when ground, were produced by GoodMills Innovation. This suggests that low-moisture extrusion conditions such as temperature, pressure, and screw speed, which were likely different between the two producers, strongly impacted cooking loss of patties. However, none of the CL-related properties correlated with the structural characteristics of TVPs. The composition of the TVPs may have contributed to the results. Therefore, the correlation analysis was extended by including the  $CL_{structure}$  (supplementary information, Equation (2)), reflecting the difference between CL for the intact and ground TVP patties. An overview of all correlation coefficients between CL-related properties of the patties and structural characteristics of TVP can be found in Table A1 in the Appendix. However, none of the corrected CL-related properties correlated with the structural features of TVPs.

Strong correlations were observed between sous-vide CL ( $r = 0.91$ ,  $p < 0.001$ ) and total CL ( $r = 0.86$ ,  $p < 0.001$ ) of patties with intact or ground TVPs, suggesting that the CL was mainly related to the material

**Table 9** Sous-vide cooking loss (CL), total CL, and water and oil loss during sous-vide cooking for patties made with intact and ground TVP. Means are reported with standard error. Means sharing superscript letters are not significantly different ( $p > 0.05$ ).

TVP type	Patties made with intact TVP				Patties made with ground TVP			
	Sous-vide CL (%)	Total CL (%)	Water loss sous-vide (%)	Oil loss sous-vide (%)	Sous-vide CL (%)	Total CL (%)	Water loss sous-vide (%)	Oil loss sous-vide (%)
	ROQ1	4.9 ± 0.1 <sup>ef</sup>	10.6 ± 0.1 <sup>f</sup>	3.7 ± 0.1 <sup>e</sup>	0.1 ± 0.0 <sup>g</sup>	1.8 ± 0.1 <sup>ab</sup>	5.9 ± 0.1 <sup>ab</sup>	1.5 ± 0.0 <sup>ab</sup>
ROQ2	4.7 ± 0.2 <sup>def</sup>	9.7 ± 0.0 <sup>cdef</sup>	3.6 ± 0.1 <sup>de</sup>	0.4 ± 0.0 <sup>a</sup>	1.8 ± 0.1 <sup>ab</sup>	6.1 ± 0.4 <sup>ab</sup>	1.5 ± 0.1 <sup>ab</sup>	0.0 ± 0.0 <sup>a</sup>
ROQ3	3.1 ± 0.0 <sup>bc</sup>	8.0 ± 0.3 <sup>b</sup>	2.1 ± 0.0 <sup>f</sup>	0.4 ± 0.0 <sup>a</sup>	1.8 ± 0.7 <sup>ab</sup>	6.1 ± 0.3 <sup>ab</sup>	1.5 ± 0.6 <sup>ab</sup>	0.0 ± 0.0 <sup>a</sup>
ROQ4	2.7 ± 0.1 <sup>b</sup>	7.9 ± 0.3 <sup>b</sup>	2.3 ± 0.1 <sup>bc</sup>	0.0 ± 0.0 <sup>a</sup>	2.4 ± 0.6 <sup>abc</sup>	6.7 ± 0.1 <sup>bc</sup>	2.0 ± 0.5 <sup>bc</sup>	0.0 ± 0.0 <sup>a</sup>
ROQ5	1.0 ± 0.1 <sup>a</sup>	5.6 ± 0.2 <sup>a</sup>	0.0 ± 0.0 <sup>a</sup>	0.0 ± 0.0 <sup>a</sup>	0.5 ± 0.0 <sup>a</sup>	4.6 ± 0.7 <sup>a</sup>	0.0 ± 0.0 <sup>a</sup>	0.0 ± 0.0 <sup>a</sup>
VEG1	3.8 ± 0.1 <sup>bcd</sup>	8.4 ± 0.3 <sup>bc</sup>	3.3 ± 0.1 <sup>de</sup>	0.0 ± 0.0 <sup>a</sup>	3.0 ± 0.0 <sup>bc</sup>	6.7 ± 0.6 <sup>bc</sup>	2.5 ± 0.0 <sup>bc</sup>	0.1 ± 0.0 <sup>ab</sup>
VEG2	4.0 ± 0.1 <sup>bcd</sup>	9.2 ± 0.2 <sup>bcde</sup>	3.4 ± 0.1 <sup>de</sup>	0.1 ± 0.0 <sup>a</sup>	6.1 ± 0.9 <sup>de</sup>	10.7 ± 0.2 <sup>d</sup>	4.8 ± 0.7 <sup>de</sup>	0.2 ± 0.0 <sup>b</sup>
GMI1	4.2 ± 0.0 <sup>cde</sup>	8.6 ± 0.1 <sup>bcd</sup>	3.6 ± 0.0 <sup>e</sup>	0.1 ± 0.0 <sup>a</sup>	4.3 ± 0.1 <sup>c</sup>	8.3 ± 0.1 <sup>c</sup>	3.6 ± 0.2 <sup>cd</sup>	0.1 ± 0.0 <sup>ab</sup>
GMI2	3.5 ± 0.1 <sup>bcd</sup>	8.1 ± 0.4 <sup>b</sup>	2.9 ± 0.1 <sup>cd</sup>	0.0 ± 0.0 <sup>a</sup>	6.4 ± 0.1 <sup>e</sup>	10.7 ± 0.2 <sup>d</sup>	5.3 ± 0.1 <sup>ef</sup>	0.1 ± 0.0 <sup>ab</sup>
GMI3	6.5 ± 0.1 <sup>g</sup>	9.9 ± 0.1 <sup>def</sup>	4.8 ± 0.0 <sup>f</sup>	1.2 ± 0.0 <sup>b</sup>	11.5 ± 0.1 <sup>g</sup>	13.6 ± 0.0 <sup>f</sup>	6.5 ± 0.0 <sup>f</sup>	4.1 ± 0.0 <sup>c</sup>
GMI4	10.3 ± 0.3 <sup>h</sup>	15.5 ± 0.4 <sup>g</sup>	7.8 ± 0.2 <sup>g</sup>	1.6 ± 0.0 <sup>b</sup>	15.1 ± 0.1 <sup>h</sup>	17.2 ± 0.1 <sup>f</sup>	10.1 ± 0.0 <sup>g</sup>	4.0 ± 0.0 <sup>c</sup>
GMI5	5.8 ± 0.7 <sup>g</sup>	10.1 ± 0.3 <sup>ef</sup>	2.0 ± 0.2 <sup>b</sup>	3.4 ± 0.4 <sup>c</sup>	8.9 ± 0.2 <sup>f</sup>	11.7 ± 0.1 <sup>d</sup>	2.6 ± 0.1 <sup>bc</sup>	5.7 ± 0.1 <sup>d</sup>
GMI6	15.1 ± 0.2 <sup>i</sup>	17.3 ± 0.2 <sup>h</sup>	9.5 ± 0.1 <sup>h</sup>	4.4 ± 0.1 <sup>d</sup>	18.3 ± 0.0 <sup>i</sup>	18.8 ± 0.2 <sup>f</sup>	11.3 ± 0.0 <sup>g</sup>	5.9 ± 0.0 <sup>d</sup>

itself, rather than the structure of TVPs. It was expected that TVPs with a higher WAC would be able to retain more water during cooking, resulting in a lower CL. However, no correlations were observed between CL and WAC (Appendix, Table A1). In contrast, Hong et al. (Hong et al., 2022) found that the CL of patties correlated with the WAC of TVP ( $r = 0.68, p < 0.01$ ). This discrepancy between studies could be explained by differences in water contents between patties as Hong et al. rehydrated TVPs up to the maximum WAC, and therefore the initial water content of the samples was different. In our study, all TVPs contained the same water content when incorporated into patties. Unfortunately, Hong et al. did not report any structural characteristics of TVPs other than bulk density which is often regarded as a measure of porosity. Bulk density did not correlate with cooking loss, which is in agreement with our findings.

The grilling step resulted in approximately 5–6% cooking loss for all patties (supplementary information, Table S2). Analysis of the cooking loss composition revealed that only six TVPs (ROQ2, ROQ3, GMI3, GMI4, GMI5 and GMI6) had a substantial oil loss. ROQ1 and ROQ2 released more oil when intact, while GMI3, GMI4, GMI5 and GMI6 released more oil when TVP was ground. Again, these differences were mostly related to the producer of the TVP, as patties that released more oil when TVPs were intact, contained TVP from Roquette (ROQ series), and patties that released more oil when TVPs were ground, contained TVP from GoodMills Innovation (GMI series). It was expected that all TVPs would exhibit less oil loss during cooking when TVPs were ground, since a higher surface area could favour accommodation of oil into small cavities within the TVP, increasing oil retention. However, as this was not the case, other properties may be more relevant. Shrinkage of patties during cooking and differences in pH (supplementary information, Table S2) were ruled out to be the origin of the differences. Therefore, the differences in cooking loss are likely caused by differences in composition of TVP, which impacts material properties such as hydrophobicity.

### 3.4.3. Expressible liquid

The expressible liquid is a measure for the serum that is released during consumption and has been correlated to the juiciness perception of meat products (C. M. Lee & Patel, 1984; Lucherik et al., 2017; Yau & Huang, 2001). Table 10 presents the expressible water (EW), expressible oil (EO) and the total expressible liquid (EL) of the grilled patties.

The type of TVP affected the EO and EL of patties with intact TVP, while the EW was not significantly different for any of the samples. Interestingly, the EL of patties with TVPs produced by GMI was generally higher than the EL of patties with TVPs produced by Roquette, pointing again to the importance of processing conditions, as mentioned in section 3.4.2. Additionally, the positive correlation between EL and total CL ( $r = 0.58, p < 0.05$ ) shows that patties with high cooking loss also tended to have higher expressible liquid. In patties with ground TVPs, TVPs from GMI also resulted in higher EL-values than those from Roquette, with an even stronger correlation with total CL ( $r = 0.85, p < 0.001$ ). This positive correlation between cooking loss and expressible liquid has been previously reported by Lee et al. (J. Lee et al., 2020) for pork patties, and indicates that systems with more liquid release during cooking also tend to release more liquid during compression.

To compare the EL values for patties with intact and ground TVP, the contribution of the structure to the EL ( $EL_{structure}$ ) was estimated using Equation S3 in the supplementary information. None of the structural characteristics of TVP correlated with the EW, EO or EL of patties with intact or ground TVPs. However, a significant negative correlation was found between  $EL_{structure}$  and the  $WHC_{structure}$  ( $r = -0.62, p < 0.01$ ), which was in agreement with our expectations. TVP structures able to retain more water under centrifugal forces (high WHC) are less likely to release this water during compression (EL). In section 3.3, it was observed that the wall thickness and porosity of TVP significantly influenced the  $WHC_{structure}$ . This suggests that, despite the lack of significant correlations with the structural features on their own, the

**Table 10**

Expressible water (EW), expressible oil (EO) and total expressible liquid (EL) of patties made with intact TVP and patties made with ground TVP. Means are reported with standard error. Means sharing superscript letters are not significantly different ( $p > 0.05$ ).

TVP type	Patties made with intact TVP			Patties made with ground TVP		
	EW (%)	EO (%)	EL (%)	EW (%)	EO (%)	EL (%)
ROQ1	2.9 ± 1.3 <sup>a</sup>	4.9 ± 0.2 <sup>abc</sup>	7.8 ± 1.1 <sup>abc</sup>	3.5 ± 0.3 <sup>a</sup>	2.2 ± 0.2 <sup>abcd</sup>	5.7 ± 0.5 <sup>a</sup>
ROQ2	3.5 ± 0.2 <sup>a</sup>	4.1 ± 0.2 <sup>ab</sup>	7.6 ± 0.4 <sup>abc</sup>	2.9 ± 0.2 <sup>a</sup>	1.8 ± 0.1 <sup>ab</sup>	4.7 ± 0.4 <sup>a</sup>
ROQ3	3.6 ± 0.0 <sup>a</sup>	4.2 ± 0.2 <sup>abc</sup>	7.8 ± 0.3 <sup>abc</sup>	3.1 ± 0.1 <sup>a</sup>	1.9 ± 0.0 <sup>abc</sup>	5.1 ± 0.1 <sup>a</sup>
ROQ4	3.0 ± 0.1 <sup>a</sup>	3.6 ± 0.0 <sup>ab</sup>	6.6 ± 0 <sup>ab</sup>	2.9 ± 0.0 <sup>a</sup>	1.4 ± 0.0 <sup>a</sup>	4.3 ± 0.1 <sup>a</sup>
ROQ5	2.5 ± 0.3 <sup>a</sup>	3.5 ± 0.2 <sup>ab</sup>	6.0 ± 0.5 <sup>a</sup>	2.9 ± 0.2 <sup>a</sup>	1.7 ± 0.3 <sup>ab</sup>	4.6 ± 0.5 <sup>a</sup>
VEG1	3.6 ± 0.1 <sup>a</sup>	3.9 ± 0.0 <sup>ab</sup>	7.5 ± 0.1 <sup>abc</sup>	3.0 ± 0.3 <sup>a</sup>	1.1 ± 0.1 <sup>a</sup>	4.1 ± 0.5 <sup>a</sup>
VEG2	4.1 ± 0.5 <sup>a</sup>	4.8 ± 0.6 <sup>abc</sup>	8.9 ± 1.1 <sup>abc</sup>	3.7 ± 0.4 <sup>a</sup>	4.2 ± 0.5 <sup>def</sup>	7.9 ± 0.9 <sup>a</sup>
GMI1	3.8 ± 0.1 <sup>a</sup>	3.3 ± 0.4 <sup>a</sup>	7.1 ± 0.6 <sup>abc</sup>	3.8 ± 0.7 <sup>a</sup>	2.9 ± 0.4 <sup>abcde</sup>	6.7 ± 1.2 <sup>a</sup>
GMI2	4.2 ± 0.2 <sup>a</sup>	4.2 ± 0.5 <sup>ab</sup>	8.4 ± 0.7 <sup>abc</sup>	3.5 ± 0.3 <sup>a</sup>	3.7 ± 0.2 <sup>bcde</sup>	7.2 ± 0.6 <sup>a</sup>
GMI3	4.7 ± 0.1 <sup>a</sup>	6.0 ± 0.1 <sup>c</sup>	10.6 ± 0.3 <sup>bc</sup>	4.4 ± 1.1 <sup>ab</sup>	4.6 ± 0.5 <sup>ef</sup>	9.1 ± 1.6 <sup>ab</sup>
GMI4	5.2 ± 0.1 <sup>a</sup>	4.9 ± 0.1 <sup>abc</sup>	10.1 ± 0.0 <sup>bc</sup>	7.0 ± 0.4 <sup>b</sup>	6.0 ± 0.2 <sup>f</sup>	13.0 ± 0.6 <sup>b</sup>
GMI5	5.5 ± 2.1 <sup>a</sup>	5.2 ± 0.4 <sup>bc</sup>	10.7 ± 1.6 <sup>c</sup>	3.3 ± 0.4 <sup>a</sup>	4.1 ± 0.8 <sup>def</sup>	7.4 ± 1.2 <sup>a</sup>
GMI6	4.2 ± 0.2 <sup>a</sup>	5.0 ± 0.4 <sup>abc</sup>	9.2 ± 0.6 <sup>abc</sup>	4.1 ± 1.0 <sup>ab</sup>	4.0 ± 0.5 <sup>cdef</sup>	8.2 ± 1.5 <sup>ab</sup>

**Table 11**

Young's modulus (E), yield stress ( $\sigma_y$ ) and yield strain ( $\epsilon_y$ ) of patties made with intact TVP and ground TVP. Means are reported with standard error. Means sharing superscript letters are not significantly different ( $p > 0.05$ ).

TVP type	Patties made with intact TVP			Patties made with ground TVP		
	E (kPa)	$\sigma_{y(TA)}$ (kPa)	$\epsilon_{y(TA)}$ (–)	E (kPa)	$\sigma_{y(TA)}$ (kPa)	$\epsilon_{y(TA)}$ (–)
ROQ1	23.9 ± 0.8 <sup>cde</sup>	19.0 ± 1.0 <sup>de</sup>	0.68 ± 0.06 <sup>bcd</sup>	14.4 ± 2.1 <sup>a</sup>	9.4 ± 0.3 <sup>b</sup>	0.48 ± 0.01 <sup>a</sup>
ROQ2	16.0 ± 0.1 <sup>abc</sup>	15.5 ± 2.4 <sup>abcd</sup>	0.66 ± 0.06 <sup>abcd</sup>	13.2 ± 2.0 <sup>a</sup>	7.4 ± 0.2 <sup>ab</sup>	0.40 ± 0.02 <sup>a</sup>
ROQ3	16.4 ± 3.7 <sup>abc</sup>	14.0 ± 1.0 <sup>abcd</sup>	0.63 ± 0.05 <sup>abc</sup>	18.2 ± 1.2 <sup>ab</sup>	9.0 ± 0.4 <sup>b</sup>	0.42 ± 0.03 <sup>a</sup>
ROQ4	9.0 ± 0.0 <sup>ab</sup>	9.0 ± 0.2 <sup>abc</sup>	0.57 ± 0.03 <sup>abc</sup>	13.0 ± 1.7 <sup>a</sup>	5.0 ± 0.2 <sup>ab</sup>	0.39 ± 0.02 <sup>a</sup>
ROQ5	15.5 ± 0.5 <sup>abc</sup>	7.3 ± 0.1 <sup>ab</sup>	0.46 ± 0.05 <sup>ab</sup>	9.2 ± 0.5 <sup>a</sup>	3.6 ± 0.1 <sup>a</sup>	0.40 ± 0.04 <sup>a</sup>
VEG1	37.0 ± 2.7 <sup>f</sup>	16.9 ± 1.4 <sup>cd</sup>	0.59 ± 0.01 <sup>abc</sup>	26.2 ± 2.1 <sup>bc</sup>	9.5 ± 0.6 <sup>b</sup>	0.48 ± 0.06 <sup>a</sup>
VEG2	12.2 ± 0.2 <sup>ab</sup>	5.9 ± 0.1 <sup>a</sup>	0.51 ± 0.04 <sup>ab</sup>	11.1 ± 1.5 <sup>a</sup>	6.2 ± 0.7 <sup>ab</sup>	0.51 ± 0.03 <sup>ab</sup>
GMI1	17.4 ± 0.8 <sup>abcd</sup>	8.4 ± 0.4 <sup>abc</sup>	0.43 ± 0.01 <sup>a</sup>	16.5 ± 1.3 <sup>ab</sup>	7.7 ± 0.3 <sup>ab</sup>	0.38 ± 0.01 <sup>a</sup>
GMI2	7.3 ± 2.0 <sup>a</sup>	–	–	13.3 ± 2.0 <sup>a</sup>	7.1 ± 0.4 <sup>ab</sup>	0.41 ± 0.05 <sup>a</sup>
GMI3 <sup>a</sup>	18.6 ± 2.5 <sup>bcd</sup>	34.7 ± 1.4 <sup>fg</sup>	0.99 ± 0.05 <sup>e</sup>	12.9 ± 1.7 <sup>a</sup>	47.6 ± 0.5 <sup>d</sup>	1.09 ± 0.08 <sup>c</sup>
GMI4	27.3 ± 3.0 <sup>def</sup>	–	–	32.1 ± 3.9 <sup>c</sup>	47.6 ± 3.0 <sup>d</sup>	0.98 ± 0.03 <sup>c</sup>
GMI5 <sup>a</sup>	19.2 ± 0.8 <sup>bcde</sup>	27.0 ± 3.0 <sup>ef</sup>	0.79 ± 0.05 <sup>cde</sup>	14.1 ± 2.2 <sup>a</sup>	22.4 ± 0.7 <sup>c</sup>	0.79 ± 0.08 <sup>bc</sup>
GMI6 <sup>a</sup>	29.3 ± 2.3 <sup>ef</sup>	39.3 ± 2.4 <sup>g</sup>	0.88 ± 0.01 <sup>de</sup>	26.3 ± 0.1 <sup>bc</sup>	49.5 ± 0.7 <sup>d</sup>	0.99 ± 0.13 <sup>c</sup>

<sup>a</sup> GMI3, GMI5 and GMI6 showed more fracture-like behaviour instead of yielding for both patties with intact TVP and the ones with ground TVP.

structure of TVP still plays a role in the expressible liquid of patties made with TVP, which is expected to impact their sensory perception.

#### 3.4.4. Textural properties of patties

The effect of TVP on the textural properties of patties was investigated using uniaxial compression tests. The Young's modulus and yielding properties determined from these experiments are presented in Table 11.

The textural properties of patties varied significantly depending on TVP type. For patties with intact TVPs, the Young's modulus ranged from 7.3 to 37.0 kPa, while the yield stress and strain ranged from 5.9 to 39.3 kPa and 0.43 to 0.99, respectively. Similarly, for patties with ground TVPs, the Young's modulus ranged from 9.2 to 32.1 kPa and the yield stress and strain from 3.6 to 49.5 kPa and 0.38 to 1.09, respectively.

When analysing patties made from intact TVPs, a negative correlation was observed between Young's modulus and MPS ( $r = -0.60$ ,  $p < 0.05$ ), indicating that smaller pores resulted in stiffer patties. This correlation became even stronger when correcting for the contribution of the material, as  $E_{\text{structure}}$  also correlated with the Young's modulus of the patties ( $r = -0.74$ ,  $p < 0.01$ ). This has not been reported for meat analogues before, and can likely be explained based on the higher rigidity of small pores compared to large pores, as previously reported by Liu (Liu, 1997) for porous ceramics and Licciardello et al. (Licciardello et al., 2012) for meringues. Additionally, these studies showed that the mean pore size influences the mechanical properties and that the level of porosity, as well as different length scales, such as micro- and macro-pores, impact mechanical properties.

Three patties (GMI3, GMI5 and GMI6) exhibited a more fracture-like

behaviour, whereas other patties showed yielding. The stress-strain curves from which this was derived are provided in the supplementary information (Figs. S1 and S2). GMI3, GMI5 and GMI6 were also the hardest ( $\sigma_{y(TA)}$ ) and the most deformable ( $\epsilon_{y(TA)}$ ) patties. As this occurred for both patties with intact TVPs and ground TVPs, it was likely not caused by the structural features of TVPs, since patties with ground TVPs lack these features. These three TVPs had relatively high protein contents compared to the other TVPs. As  $\sigma_{y(TA)}$  and  $\epsilon_{y(TA)}$  of patties with intact TVP correlated with protein content ( $\sigma_{y(TA)}$ :  $r = 0.73$ ,  $p < 0.05$  and  $\epsilon_{y(TA)}$ :  $r = 0.75$ ,  $p < 0.01$ ), the additional protein in GMI3, GMI5 and GMI6 may have contributed to increased texturisation, harder TVP chunks, and thereby harder patties. This is in line with previous studies that showed a correlation between protein content and both hardness and breaking strength of extrudates (Allen et al., 2007; Onwulata & Konstance, 2006; Yadav et al., 2014). The relatively high deformability of GMI3, GMI5 and GMI6 compared to the other TVPs was unexpected, as materials with high deformability (low brittleness) are usually less likely to fracture. However, patties are complex, heterogeneous systems that include air pockets, and therefore possess many microstructural features that can lead to stress concentration, and thereby affecting fracture behaviour. Hence, the high deformability of GMI3, GMI5 and GMI6 may be a result of various structural features.

## 4. Conclusions

In this study, we investigated the relationships between the structural characteristics of commercial TVPs and (a) their rehydration behaviour, and (b) the mechanical properties and serum release (cooking loss and expressible liquid) of patties prepared with these TVPs. The

utilisation of X-ray microtomography facilitated a comprehensive exploration of the structural characteristics of TVPs produced with low-moisture extrusion. Water absorption by TVPs was described well by a two-term exponential model, demonstrating the presence of a fast and slow water uptake process. On short time scales, thick walls were able to transport more water than thin walls, resulting in a higher initial water uptake rate. However, the maximum water absorption capacity and the water holding capacity positively correlated with porosity, while wall thickness had a negative effect.

When patties were prepared from TVPs, correlations between structural features of TVP and the different properties of patties were generally weak. This may be attributed to the partial breakdown of these structural features during patty preparation. However, thicker walls and smaller pores resulted in stiffer patty batters and stiffer grilled patties, respectively. The serum release could not be explained by any of the structural characteristics of TVP, although patties with more release during cooking, also released more serum during compression. The serum release features may thus be more related to the composition of the TVP. Furthermore, large differences were found in functional properties between TVPs from different producers, emphasizing the importance of processing conditions.

Overall, our study demonstrated how structural characteristics of TVPs such as porosity and wall thickness facilitate water absorption and water holding capacity. This study did not explore the effect of TVP composition in detail, although this may explain some of the properties of the patties. Therefore, future studies should explore TVPs with the same composition, to verify some of the relations with structural features only. Such additional insights may reveal important structural characteristics of TVPs, and could help to optimise the production processes of TVPs.

Appendix A. Supplementary data

Supplementary data to this article can be found online at <https://doi.org/10.1016/j.foodhyd.2023.109529>.

Appendix

Table A1

Correlation matrix of TVP properties and cooking loss (CL) and expressible liquid (EL)

Type of sample	Parameter	$\Phi_{XRT}$	MPS	$\sigma_{PS}^2$	MWT	$\sigma_{WT}^2$	$\rho_{wall}$	$\rho_{app}$	$\Phi_{density}$	Protein content	Bound water	WAC
Intact TVP patties	<i>Sous-vide CL</i>	0.00	-0.25	-0.23	-0.21	-0.26	0.17	0.05	-0.07	0.52	0.02	-0.28
	<i>Total CL</i>	0.10	-0.19	-0.22	-0.20	-0.22	0.23	0.01	-0.04	0.53	-0.00	-0.22
Ground TVP patties	<i>Sous-vide CL</i>	-0.10	-0.13	-0.10	-0.11	-0.17	0.11	0.11	-0.11	0.36	-0.16	-0.27
	<i>Total CL</i>	-0.09	-0.04	-0.04	-0.07	-0.12	0.11	0.11	-0.11	0.28	-0.24	-0.27
Contribution of structure	<i>Sous-vide CL</i>	0.21	-0.07	-0.10	-0.06	0.01	0.00	-0.16	0.14	-0.05	0.35	0.18
	<i>Total CL</i>	0.29	-0.17	-0.22	-0.13	-0.06	0.09	-0.19	0.15	0.16	0.43	0.20
Intact TVP patties	<i>Sous-vide water loss</i>	0.06	-0.15	-0.17	-0.20	-0.24	0.14	-0.01	0.00	0.40	-0.10	-0.21
	<i>Sous-vide oil loss</i>	-0.17	-0.33	-0.26	-0.13	-0.18	0.17	0.19	-0.23	0.55	-0.01	-0.36
Ground TVP patties	<i>Sous-vide water loss</i>	-0.03	0.02	0.02	-0.10	-0.15	0.05	0.03	-0.02	0.22	-0.29	-0.19
	<i>Sous-vide oil loss</i>	-0.16	-0.36	-0.29	-0.15	-0.20	0.17	0.19	-0.21	<b>0.56*</b>	-0.03	-0.31
Contribution of structure	<i>Sous-vide water loss</i>	0.17	-0.28	-0.31	-0.10	-0.05	0.11	-0.09	0.06	0.15	0.49	0.07
	<i>Sous-vide oil loss</i>	0.13	0.33	0.27	0.14	0.19	-0.13	-0.14	0.14	-0.48	0.05	0.20
Intact TVP patties	<i>EL-water</i>	-0.13	0.06	0.06	-0.09	-0.13	0.24	0.24	-0.24	0.18	-0.15	-0.21
	<i>EL-oil</i>	-0.02	-0.15	-0.15	-0.03	-0.04	0.31	0.18	-0.19	0.44	-0.05	-0.27
	<i>EL-total</i>	-0.08	-0.04	-0.04	-0.07	-0.10	0.30	0.23	-0.24	0.33	-0.12	-0.26
Ground TVP patties	<i>EL-water</i>	0.24	0.01	-0.07	-0.25	-0.22	0.09	-0.14	0.15	0.30	-0.16	0.11
	<i>EL-oil</i>	0.05	0.12	0.05	-0.03	-0.01	0.19	0.07	-0.05	0.11	-0.43	-0.19
	<i>EL-total</i>	0.13	0.07	0.00	-0.13	-0.11	0.16	-0.02	0.03	0.20	-0.33	-0.07
Contribution of structure	<i>EL-water</i>	-0.42	0.05	0.14	0.22	0.14	0.13	0.41	-0.42	-0.19	0.04	-0.34
	<i>EL-oil</i>	-0.08	-0.26	-0.18	0.02	-0.01	-0.05	0.03	-0.06	0.15	0.54	0.08
	<i>EL-total</i>	-0.28	-0.15	-0.04	0.13	0.07	0.03	0.25	-0.27	0.00	0.39	-0.13

\* = significance up to p < 0.05.

CRediT authorship contribution statement

**Thiemo van Esbroeck:** Conceptualization, Methodology, Investigation, Data curation, Validation, Visualization, Writing – original draft. **Guido Sala:** Conceptualization, Methodology, Validation, Supervision, Writing – review & editing. **Markus Stieger:** Conceptualization, Methodology, Validation, Supervision, Writing – review & editing, Funding acquisition. **Elke Scholten:** Conceptualization, Methodology, Validation, Supervision, Writing – review & editing, Funding acquisition.

Declaration of competing interest

The authors declare that they have no known competing financial interests or personal relationships that could have appeared to influence the work reported in this paper.

Data availability

Data will be made available on request.

Acknowledgements

This research was performed within the framework of the public-private partnership project “Improving Sensory Quality of Meat Analogues”. The project is funded by the Top Sector Agri & Food (TKI, grant number LWV-20.078) and a consortium of partners (AAK, GoodMills Innovation, Starfield, Symrise and Vivera). We thank Remco Hamoen and Maaikie Nieuwland for technical support of XRT measurements, performed on X-Ray Tomography equipment owned by Shared Research Facilities of WUR, and subsidised by the Ministry of Economic Affairs and the province of Gelderland, The Netherlands.

Table A2

Correlation matrix of TVP properties and rheological properties of patty batter and textural properties of grilled patties.

Type of sample	Parameter	$\Phi_{XRT}$	MPS	$\sigma_{PS}^2$	MWT	$\sigma_{WT}^2$	$\rho_{wall}$	$\rho_{app}$	$\Phi_{density}$	Protein content	Bound water	WAC
Intact TVP patty batter	Yield stress (rheo)	0.37	0.53	0.26	0.17	0.33	-0.13	-0.29	0.28	-0.24	0.12	0.39
	Yield strain (rheo)	-0.30	-0.19	-0.06	0.08	-0.01	-0.09	0.14	-0.16	0.19	-0.30	-0.35
Ground TVP patty batter	Yield stress (rheo)	0.35	0.07	0.17	-0.49	-0.48	-0.43	-0.47	0.48	0.08	0.50	<b>0.71**</b>
	Yield strain (rheo)	-0.20	-0.44	-0.48	0.22	0.29	-0.01	0.11	-0.15	0.24	-0.14	-0.38
Contribution of structure	Yield stress (rheo)	-0.10	0.42	0.07	<b>0.70**</b>	<b>0.80**</b>	0.31	0.28	-0.28	-0.46	-0.39	-0.30
	Yield strain (rheo)	-0.03	0.37	<b>0.58*</b>	-0.16	-0.31	-0.10	-0.01	0.04	-0.19	-0.15	0.18
Intact TVP patties	Young's modulus	-0.22	<b>-0.60*</b>	-0.51	-0.31	-0.43	0.45	0.39	-0.41	<b>0.56*</b>	<b>0.62*</b>	-0.06
	Yield stress (TA)	0.08	-0.41	-0.36	-0.37	-0.40	0.15	-0.01	-0.01	<b>0.73*</b>	0.24	-0.07
	Yield strain (TA)	0.19	-0.32	-0.27	-0.41	-0.40	0.04	-0.15	0.12	<b>0.75**</b>	0.23	0.02
Ground TVP patties	Young's modulus	0.01	-0.14	-0.12	-0.37	-0.44	0.11	0.05	-0.07	0.46	0.38	0.20
	Yield stress (TA)	0.00	-0.33	-0.27	-0.30	-0.34	0.04	-0.01	0.00	0.54	0.04	-0.14
	Yield strain (TA)	-0.09	-0.38	-0.31	-0.23	-0.28	0.13	0.11	-0.12	0.49	-0.03	-0.23
Contribution of structure	Young's modulus	-0.17	<b>-0.74**</b>	<b>-0.68*</b>	-0.05	-0.07	0.52	0.37	-0.38	0.34	0.39	-0.26
	Yield stress (TA)	0.22	-0.35	-0.35	-0.08	-0.02	0.03	-0.18	0.13	0.14	0.44	0.23
	Yield strain (TA)	0.55	0.16	0.15	-0.27	-0.16	<b>-0.46*</b>	<b>-0.67*</b>	0.64	0.11	0.38	0.53

\* = Significance up to  $p < 0.05$ , \*\* = significance up to  $p < 0.01$ .

## References

- Agbisit, R., Alavi, S., Cheng, E., Herald, T., & Trater, A. (2007). Relationships between microstructure and mechanical properties of cellular cornstarch extrudates. *Journal of Texture Studies*, 38, 199–219. <https://doi.org/10.1111/j.1745-4603.2007.00094.x>
- Allen, K. E., Carpenter, C. E., & Walsh, M. K. (2007). Influence of protein level and starch type on an extrusion-expanded whey product. *International Journal of Food Science and Technology*, 42(8), 953–960. <https://doi.org/10.1111/J.1365-2621.2006.01316.X>
- Attwood, S., & Hajat, C. (2020). How will the COVID-19 pandemic shape the future of meat consumption? *Public Health Nutrition*, 23(17), 3116–3120. <https://doi.org/10.1017/S136898002000316X>
- Barrett, A. H., & Peleg, M. (1992). Extrudate cell structure-texture relationships. *Journal of Food Science*, 57(5), 1253–1257. <https://doi.org/10.1111/J.1365-2621.1992.TB11311.X>
- Beck, S. M., Knoerzer, K., Foerster, M., Mayo, S., Philipp, C., & Arcot, J. (2018). Low moisture extrusion of pea protein and pea fibre fortified rice starch blends. *Journal of Food Engineering*, 231, 61–71. <https://doi.org/10.1016/J.JFOODENG.2018.03.004>
- Boukid, F. (2020). Plant-based meat analogues: From niche to mainstream. *European Food Research and Technology*, 247(2), 297–308. <https://doi.org/10.1007/S00217-020-03630-9>
- Brishti, F. H., Chay, S. Y., Muhammad, K., Ismail-Fitry, M. R., Zarei, M., & Saari, N. (2021). Texturized mung bean protein as a sustainable food source: Effects of extrusion on its physical, textural and protein quality. *Innovative Food Science and Emerging Technologies*, 67. <https://doi.org/10.1016/j.ifset.2020.102591>
- Chanvrier, H., Nordström Pillin, C., Vandeputte, G., Haiduc, A., Leloup, V., & Gumy, J. C. (2015). Impact of extrusion parameters on the properties of rice products: A physicochemical and X-ray tomography study. *Food Structure*, 6, 29–40. <https://doi.org/10.1016/J.FOOSTR.2015.06.004>
- Cheah, I., Sadat Shimul, A., Liang, J., & Phau, I. (2020). Drivers and barriers toward reducing meat consumption. *Appetite*, 149, Article 104636. <https://doi.org/10.1016/J.APPET.2020.104636>
- Chen, F. L., Wei, Y. M., & Zhang, B. (2010). Characterization of water state and distribution in textured soybean protein using DSC and NMR. *Journal of Food Engineering*, 100(3), 522–526. <https://doi.org/10.1016/J.JFOODENG.2010.04.040>
- Chiang, J. H., Tay, W., Ong, D. S. M., Liebl, D., Ng, C. P., & Henry, C. J. (2021). Physicochemical, textural and structural characteristics of wheat gluten-soy protein composited meat analogues prepared with the mechanical elongation method. *Food Structure*, 28, Article 100183. <https://doi.org/10.1016/j.foost.2021.100183>
- Dagevos, H., & Verbeke, W. (2022). Meat consumption and flexitarianism in the low countries. *Meat Science*, 192, Article 108894. <https://doi.org/10.1016/j.meatsci.2022.108894>
- Dagevos, H., & Voordouw, J. (2013). Sustainability and meat consumption: Is reduction realistic? *Sustainability: Science, Practice and Policy*, 9(2), 60–69. <https://doi.org/10.1080/15487733.2013.11908115>
- De Backer, C. J. S., & Hudders, L. (2014). *Ecology of food and nutrition from meatless Mondays to meatless Sundays: Motivations for meat reduction among vegetarians and semi-vegetarians who mildly or significantly reduce their meat intake*. <https://doi.org/10.1080/03670244.2014.896797>
- de Gennes, P.-G., Brochard-Wyart, F., & Quéré, D. (2004). *Capillarity and wetting phenomena* (pp. 33–67). New York: Springer. [https://doi.org/10.1007/978-0-387-21656-0\\_2](https://doi.org/10.1007/978-0-387-21656-0_2)
- Elzerman, J. E., Hoek, A. C., van Boekel, M. A. J. S., & Luning, P. A. (2011). Consumer acceptance and appropriateness of meat substitutes in a meal context. *Food Quality and Preference*, 22(3), 233–240. <https://doi.org/10.1016/J.FOODQUAL.2010.10.006>
- European Commission. (2005). Attitudes of consumers towards the welfare of farmed animals. In *Eurobarometer*.
- Ganesan, K., Barowski, A., Ratke, L., & Milow, B. (2019). Influence of hierarchical porous structures on the mechanical properties of cellulose aerogels. *Journal of Sol-Gel Science and Technology*, 89, 156–165. <https://doi.org/10.1007/s10971-018-4828-2>
- Gibson, L. J., & Ashby, M. F. (1997). *Cellular solids: Structure and properties*. Cambridge University Press. <https://doi.org/10.1017/CBO9781139878326>
- Guillemic, R. M., Aksoy, E. C., Aritan, S., Erkinbaev, C., Paliwal, J., & Koksels, F. (2021). X-Ray microtomography imaging of red lentil puffed snacks: Processing conditions, microstructure and texture. *Food Research International*, 140. <https://doi.org/10.1016/J.FOODRES.2020.109996>
- Hales, T. C. (2006). Historical overview of the Kepler conjecture. *Discrete & Computational Geometry*, 36(1), 5–20. <https://doi.org/10.1007/s00454-005-1210-2>
- Hamdaoui, M., Achour, N. S., & Ben Nasrallah, S. (2014). The influence of woven fabric structure on kinetics of water sorption. *Journal of Engineered Fibers and Fabrics*, 9(1), 101–106.
- Hayashi, N., Hayakawa, I., & Fujio, Y. (1992). Hydration of heat-treated soy protein isolate and its effect on the molten flow properties at an elevated temperature. *International Journal of Food Science and Technology*, 27, 565–571. <https://doi.org/10.1111/j.1365-2621.1992.tb01223.x>
- Henderson, S. M. (1974). Progress in developing the thin layer drying equation. *Transactions of the American Society of Agricultural Engineers*, 17(6), 1167–1168.
- Hodge, R. M., Edward, G. H., & Simon, G. P. (1996). Water absorption and states of water in semicrystalline poly(vinyl alcohol) films. *Polymer*, 37(8), 1371–1376. [https://doi.org/10.1016/0032-3861\(96\)81134-7](https://doi.org/10.1016/0032-3861(96)81134-7)
- Hoek, A. C., Luning, P. A., Weijzen, P., Engels, W., Kok, F. J., & de Graaf, C. (2011). Replacement of meat by meat substitutes. A survey on person- and product-related factors in consumer acceptance. *Appetite*, 56(3), 662–673. <https://doi.org/10.1016/J.APPET.2011.02.001>
- Hong, S., Shen, Y., & Li, Y. (2022). Physicochemical and functional properties of texturized vegetable proteins and cooked patty textures: Comprehensive characterization and correlation analysis. *Foods*, 11(17). <https://doi.org/10.3390/FOODS11172619>
- Ismail, I., Hwang, Y. H., & Joo, S. T. (2020). Meat analog as future food: A review. *Journal of Animal Science And Technology*, 62(2), 111–120. <https://doi.org/10.5187/jast.2020.62.2.111>
- Joshi, V. K., & Kumar, S. (2015). Meat Analogues: Plant based alternatives to meat products - a review. *International Journal of Food and Fermentation Technology*, 5(2), 107–119. <https://doi.org/10.5958/2277-9396.2016.00001.5>
- Kachrimanis, K., Noisternig, M. F., Griesser, U. J., & Malamataris, S. (2006). Dynamic moisture sorption and desorption of standard and silicified microcrystalline cellulose. *European Journal of Pharmaceutics and Biopharmaceutics*, 64(3), 307–315. <https://doi.org/10.1016/J.EJPB.2006.05.019>
- Karizaki, V. M. (2016). Kinetic modeling and determination of mass transfer parameters during cooking of rice. *Innovative Food Science & Emerging Technologies*, 38, 131–138. <https://doi.org/10.1016/J.IFSET.2016.09.017>
- Kohler, R., Dück, R., Ausperger, B., & Alex, R. (2003). A numeric model for the kinetics of water vapor sorption on cellulosic reinforcement fibers. *Composite Interfaces*, 10, 255–276. <https://doi.org/10.1163/156855403765826900>

- Kyriakopoulou, K., Keppler, J. K., & van der Goot, A. J. (2021). Functionality of ingredients and additives in plant-based meat analogues. *Foods*, 10(3). <https://doi.org/10.3390/foods10030600>. MDPI AG.
- Lacroix, K., & Gifford, R. (2019). Reducing meat consumption: Identifying group-specific inhibitors using latent profile analysis. *Appetite*, 138, 233–241. <https://doi.org/10.1016/J.APPET.2019.04.002>
- Lee, J., Kim, H., Choi, M. J., & Cho, Y. (2020). Improved physicochemical properties of pork patty supplemented with oil-in-water nanoemulsion. *Food Science of Animal Resources*, 40(2), 262–273. <https://doi.org/10.5851/KOSFA.2020.E11>
- Lee, J.-S., Oh, H., Choi, I., Yoon, C. S., & Han, J. (2022). Physico-chemical characteristics of rice protein-based novel textured vegetable proteins as meat analogues produced by low-moisture extrusion cooking technology. *LWT - Food Science and Technology*, 157, Article 113056. <https://doi.org/10.1016/j.lwt.2021.113056>
- Lee, C. M., & Patel, K. M. (1984). Analysis of juiciness of commercial frankfurters. *Journal of Texture Studies*, 15(1), 67–73. <https://doi.org/10.1111/J.1745-4603.1984.TB00368.X>
- Lenth, R. V. (2023). *Package 'emmeans'*.
- Licciardello, F., Frisullo, P., Laverse, J., Muratore, G., & Del Nobile, M. A. (2012). Effect of sugar, citric acid and egg white type on the microstructural and mechanical properties of meringues. *Journal of Food Engineering*, 108(3), 453–462. <https://doi.org/10.1016/J.JFOODENG.2011.08.021>
- Liu, D. M. (1997). Influence of porosity and pore size on the compressive strength of porous hydroxyapatite ceramic. *Ceramics International*, 23(2), 135–139. [https://doi.org/10.1016/S0272-8842\(96\)00009-0](https://doi.org/10.1016/S0272-8842(96)00009-0)
- Lucher, L. W., O'Quinn, T. G., Legako, J. F., Rathmann, R. J., Brooks, J. C., & Miller, M. F. (2017). Assessment of objective measures of beef steak juiciness and their relationships to sensory panel juiciness ratings. *Journal of Animal Science*, 95(6), 2421–2437. <https://doi.org/10.2527/JAS.2016.0930>
- Luo, S., Chan, E., Masatcioglu, M. T., Erkinbaev, C., Paliwal, J., & Koksel, F. (2020). Effects of extrusion conditions and nitrogen injection on physical, mechanical, and microstructural properties of red lentil puffed snacks. *Food and Bioprocess Technology*, 12(1), 143–153. <https://doi.org/10.1016/J.FBP.2020.02.002>
- Mayfield, L. E., Bennett, R. M., Tranter, R. B., & Wooldridge, M. J. (2007). Consumption of welfare-friendly food products in Great Britain, Italy and Sweden, and how it may be influenced by consumer attitudes to, and behaviour towards, animal welfare attributes. *International Journal of Sociology of Food and Agriculture*, 15(3), 59–73. <https://doi.org/10.48416/IJSAF.V15I3.284>
- McEachern, M. G., & Schröder, M. J. A. (2002). The role of livestock production ethics in consumer values towards meat. *Journal of Agricultural and Environmental Ethics*, 15(2), 221–237. <https://doi.org/10.1023/A:1015052816477>
- Ning, L., & Villota, R. (1994). Influence of 7S and 11S globulins on the extrusion performance of soy protein concentrates. *Journal of Food Processing and Preservation*, 18(5), 421–436. <https://doi.org/10.1111/J.1745-4549.1994.TB00263.X>
- Okubayashi, S., Griesser, U. J., & Bechtold, T. (2004). A kinetic study of moisture sorption and desorption on lyocell fibers. *Carbohydrate Polymers*, 58(3), 293–299. <https://doi.org/10.1016/J.CARBPOL.2004.07.004>
- Okubayashi, S., Griesser, U. J., & Bechtold, T. (2005). Moisture sorption/desorption behavior of various manmade cellulosic fibers. *Journal of Applied Polymer Science*, 97(4), 1621–1625. <https://doi.org/10.1002/APP.21871>
- Onwulata, C. I., & Konstance, R. P. (2006). Extruded corn meal and whey protein concentrate: Effect of particle size. *Journal of Food Processing and Preservation*, 30, 475–487. <https://doi.org/10.1111/j.1745-4549.2005.00082.x>
- Peleg, M. (1988). An empirical model for the description of moisture sorption curves. *Journal of Food Science*, 53(4), 1216–1217. <https://doi.org/10.1111/j.1365-2621.1988.tb13565.x>
- Rucker-Gramm, P., & Beddoe, R. E. (2010). Effect of moisture content of concrete on water uptake. *Cement and Concrete Research*, 40(1), 102–108. <https://doi.org/10.1016/J.CEMCONRES.2009.09.001>
- Samard, S., Gu, B. Y., & Ryu, G. H. (2019). Effects of extrusion types, screw speed and addition of wheat gluten on physicochemical characteristics and cooking stability of meat analogues. *Journal of the Science of Food and Agriculture*, 99(11), 4922–4931. <https://doi.org/10.1002/JSFA.9722>
- Samard, S., Maung, T. T., Gu, B. Y., Kim, M. H., & Ryu, G. H. (2021). Influences of extrusion parameters on physicochemical properties of textured vegetable proteins and its meatless burger patty. *Food Science and Biotechnology*, 30(3), 395–403. <https://doi.org/10.1007/s10068-021-00879-y>
- Samard, S., & Ryu, G. H. (2019a). A comparison of physicochemical characteristics, texture, and structure of meat analogue and meats. *Journal of the Science of Food and Agriculture*, 99(6), 2708–2715. <https://doi.org/10.1002/JSFA.9438>
- Samard, S., & Ryu, G. H. (2019b). Physicochemical and functional characteristics of plant protein-based meat analogs. *Journal of Food Processing and Preservation*, 43(10). <https://doi.org/10.1111/JFPP.14123>
- Steinfeld, H., Gerber, P., Wassenaar, T., Castel, V., Rosales, M., & de Haan, C. (2006). *Livestock's long shadow: Environmental issues and options. In Food and agriculture organization of the united nations.*
- Tang, X., De Rooij, M. R., van Duynhoven, J., & van Breugel, K. (2008). Dynamic volume change measurements of cereal materials by environmental scanning electron microscopy and videomicroscopy. *Journal of Microscopy*, 230, 100–107. <https://doi.org/10.1111/j.1365-2818.2008.01962.x>
- Tuohy, J. J. (1980). Physical properties of textured whey protein II. Bulk density, water binding capacity and protein solubility. *Irish Journal of Food Science & Technology*, 4(2), 111–123.
- Vishwakarma, R. K., Shivhare, U. S., & Nanda, S. K. (2013). Water absorption kinetics of guar seeds and unhulled guar splits. *Food and Bioprocess Technology*, 6(5), 1355–1364. <https://doi.org/10.1007/S11947-012-0820-Y/FIGURES/5>
- Yadav, D. N., Anand, T., & Singh, A. K. (2014). Co-extrusion of pearl millet-whey protein concentrate for expanded snacks. *International Journal of Food Science and Technology*, 49(3), 840–846. <https://doi.org/10.1111/ijfs.12373>
- Yang, Z., Niksiar, P., & Meng, Z. (2022). Identifying structure-property relationships of micro-architected porous scaffolds through 3D printing and finite element analysis. *Computational Materials Science*, 202, Article 110987. <https://doi.org/10.1016/J.COMMATSCI.2021.110987>
- Yau, N. J. N., & Huang, Y. J. (2001). Effect of thawing methods on textural quality of sous-vide stewed beef assessed by sensory and instrumental analysis. *Journal of Food Quality*, 24(5), 375–387. <https://doi.org/10.1111/j.1745-4557.2001.tb00617.x>
- Yu, L., Ramaswamy, H. S., & Boye, J. (2013). Protein rich extruded products prepared from soy protein isolate-corn flour blends. *LWT - Food Science and Technology*, 50(1), 279–289. <https://doi.org/10.1016/J.LWT.2012.05.012>
- Zhou, R., Mitra, P., Melnychenko, A., & Rizvi, S. S. H. (2021). Quality attributes and rheological properties of novel high milk protein-based extrudates made by supercritical fluid extrusion. *International Journal of Food Science and Technology*, 56, 3866–3875. <https://doi.org/10.1111/ijfs.15003>
- Zou, Y., Zhang, W., Chen, H., & Cheng, H. (2022). Investigating the moisture absorption behavior of bamboo fiber-reinforced epoxy composites by modelling. *Bioresources*, 18(1), 272–290. <https://doi.org/10.15376/BIORES.18.1.272-290>